UNIVERSITY OF OKLAHOMA

GRADUATE COLLEGE

A DFT STUDY OF THE CATALYTIC HYDRODEOXYGENATION OF ANISOLE

ON A RHODIUM CATALYST

A THESIS

SUBMITTED TO THE GRADUATE FACULTY

in partial fulfillment of the requirements for the

Degree of

MASTER OF SCIENCE

By

DARIUS KATONO ARUHO
Norman, Oklahoma
2018

A DFT STUDY OF THE CATALYTIC HYDRODEOXYGENATION OF ANISOLE
ON A RHODIUM CATALYST

A THESIS APPROVED FOR THE
SCHOOL OF CHEMICAL, BIOLOGICAL AND MATERIALS ENGINEERING

BY

_____
Dr. Bin Wang, Chair

_____
Dr. Lance Lobban

_____
Dr. Daniel Resasco

Dedication

To my mother, siblings, professors and mentors.
Thank you.

Acknowledgements

Where do I begin? I would like to thank my advisor, ***Dr. Bin Wang***, for his guidance and support throughout my masters program, and especially for accepting me at a time that was both very difficult financially and emotionally for me. It was an honor to be among his very first master's students at the University of Oklahoma.

I would also like to thank my committee members, ***Dr. Lance Lobban*** *and* ***Dr. Daniel Resasco***, for their contributions to my work. Through their curiosity and inquisitive questioning, I have learned a lot more in graduate school than I have in previous years, especially in regards to independent thinking.

I would like to thank my office-mates and friends: Tong, Reda, Dom, Michael, Redwan, Yara, Eli, Jack, and Nhung for being a great support group.

I would like to thank my parents, mentors, family friends in Norman, and all names I can not list here, for making me feel at home in Norman.

Table of Contents

List of Tables

List of Figures

ix

Abstract

Heterogeneous catalysis is an integral part of chemical industry. Additionally, the surge in biomass research has necessitated a need for newer and effective catalysts to upgrade biomass and its constituents: - lignin, hemicellulose and cellulose. In this investigation, a refining technique of hydrodeoxygenation was investigated. Reactions of a lignin-derivative anisole were studied over monometallic Rh(111) and Rh(533) surfaces. Periodic and first-principle calculations based on density functional theory (DFT) were carried out to study surface adsorption, reaction pathways and barriers and stability of reactants and products. A terraced Rh(111) surface, whose atoms are highly coordinated, and saturated was a good model for large particles that tend to have more extended flat surfaces. Stepped Rh(533), on the other hand, modeled smaller particle catalysts that are more likely to have defects, kinks and edges on their surfaces.

In agreement with comparatives experimental studies in the literature on Pt, Ru, Fe close-packed surfaces, cleavage of $C_{aromatic}$ —O bond on anisole for both Rh(111) and Rh(533) surfaces is not possible with very high energy barriers of 226 and 141 kJ/mol, respectively. The lone pairs on oxygen atom in $C_{aromatic}$ —O are in resonance with the ring, and this π- conjugation makes the bond difficult to cleave. Results on both surfaces also showed that direct demethylation of anisole is not possible either, but instead anisole dehydrogenates successively at the —CH_3 group, until the barrier to cleave the —CH_x is low enough. The values for demethylation were calculated as 143 and 27 kJ/mol for Rh(111) and Rh(533) surfaces, respectively. Once the —CH_3 was cleaved, a phenoxy intermediate remains that waits to either be deoxygenated or

hydrogenated leading to varied selectivity. Our investigation showed that Rh(111) facilitates more hydrogenation, while Rh(533) more likely results in the deoxygenation of the surface phenoxy intermediate. It was further shown that oxygen adsorption is a descriptor for deoxygenation catalytic activity.

Chapter 1: Introduction

1.1. Overview of biomass upgrading

Environmental concerns and the uneven distribution of fossil fuel sources across the globe have prompted research into alternate energy sources such as solar, biomass, wind among others. Biomass remains as the only renewable carbon source. With the demand increase of energy and chemicals, the fraction of biomass-derived chemicals, energy and fuels is expected to increase. The U.S Department of Agriculture and U.S department of Energy set an ambitious goal to derive 20% of transportation fuels and 25% of U.S chemical commodities from biomass by 2030[4]. Via fast pyrolysis, the biomass is rapidly heated in the absence of oxygen to produce a condensable mixture of oxygenates along with char and light gases[5, 6]. The products of pyrolysis, however, do vary in percent weight depending on biomass source. Just behind cellulose, the biopolymer lignin shown in Fig. 1 is one of the three major components of biomass that is a potential source of valuable renewable organic resources. As a highly complex, high molecular weight and insoluble organic polymer, lignin presents challenges to depolymerize in order to take advantage of its many methocyclated derivatives. Most of the lignin generated from the bio-refinery process or the pulp and paper industry is currently underutilized[7].

In fact, despite the many decades spent on studying lignin, researchers have yet to fully understand its synthesis in plants cells. For long, it was believed that lignin is assembled at random to produce the highly complex cross links but now, it is

increasingly being understood that lignin has specific sequences of monolignols that suit its functions in plant cell wall[8, 9].
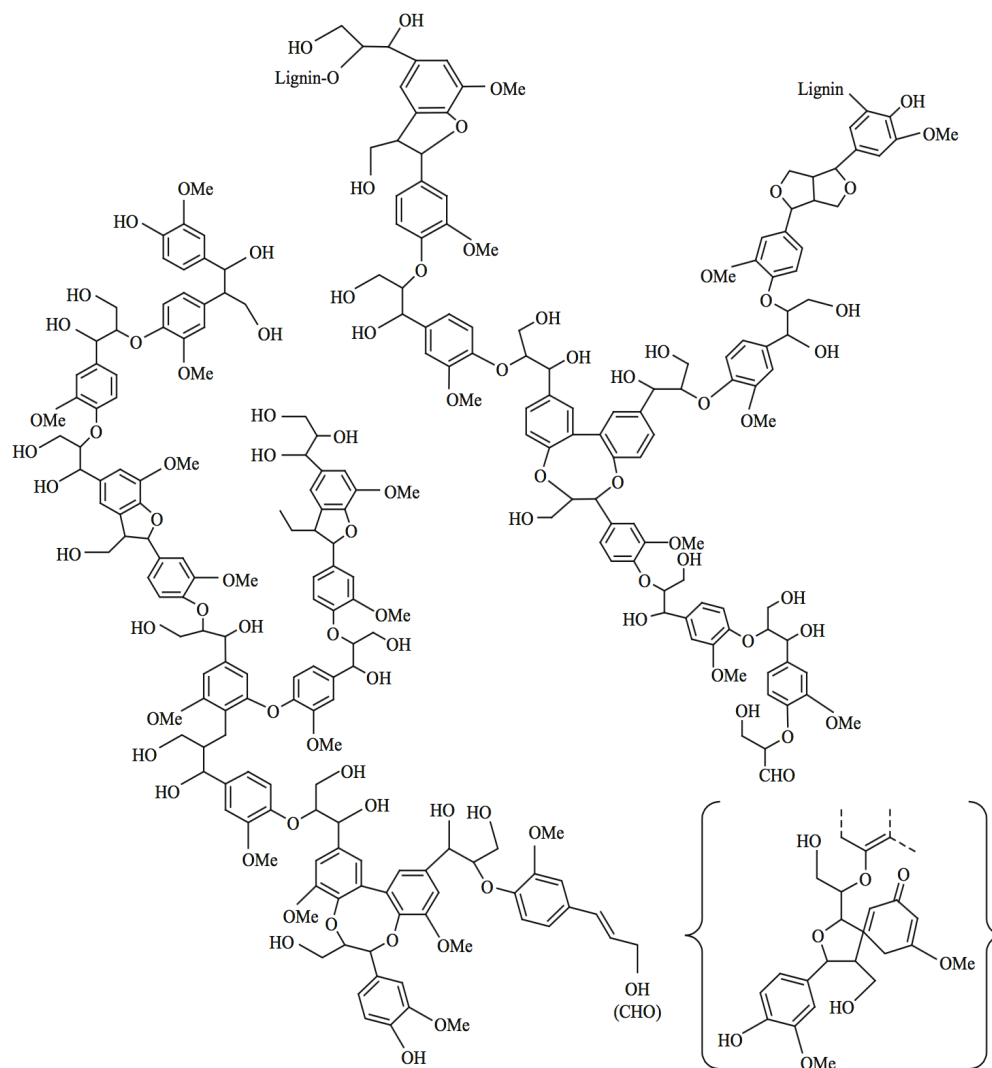
Figure 1. Complexity of lignin structure [10]

Most vividly, as shown in Fig. 1, lignin comprises numerous ether (C—O—C) linkages, a few hydroxyls (–OH) and numerous C—C bonds. There are not a lot of structures of this level of complexity.

Unlike its cellulose and hemicellulose, the sister components of lignin in plant cell walls, which are three-dimensional, crystalline and are held together by glycosydic bonds, lignin is highly amorphous, inhomogeneous and non-linear[11, 12]. More importantly, lignin is the only highly aromatic renewable resource that can be directly converted to high quality fuels[4, 13].

1.2. Problem description and motivation

Selectively converting the biomass-derived compounds into valuable chemicals is desirable to increase the economic impact of biomass conversion. As discussed above, because of the complex atomic structure of lignin with varied functionality, its thermal decomposition results in a set of compounds with varied oxygen-related functionality. A key problem is to controllably break and form chemical bonds in these compounds to convert them into valuable chemicals. Fundamental understanding of the general principles governing the bond dynamics is thus very valuable, not only to understand the reaction mechanism but also to guide exploration of alternative catalysts.

Therefore, in the scope of this thesis, a detailed study of the surface atomic and molecular adsorption and reactions for the hydrodeoxygenation of anisole (methoxybenzene) will be presented. Also, understanding of the fundamental catalytic chemistry into terraced and defected surfaces will be studied to tailor catalyst formulations to selectively convert the lignin model compounds to desired higher value products.

As discussed before, C—O bonds are abundant is biomass constituents, and their cleavage is undoubtedly a challenge even on the most oxophilic catalysts such as Fe. A significant goal in this thesis is to provide explanations for experimentally observed phenomena for hydrodeoxygenation of anisole and to establish principles for designing catalysts with high selectivity.

Chapter 2. Literature review

Numerous Studies have carried out on hydrodeoxygenation (HDO) using model compounds of lignin such as anisole, m-cresol, guacaol and have showed significant steps towards practical ways to upgrade it [14-16]. Other HDO models include furans, dimers, carboxylic acids and carbohydrates that have garnered a lot of interest and research to understand the intrinsic mechanisms [17-19].

2.1. Oxophilicity

Q. Tan and N. Duong postulated that metal oxophilicity is a good descriptor for the corresponding metal HDO activity[14][8]. Either changing the type of metal, such as from Pt, Fe, Rh, or the coordination of the metal atoms can alter the oxophilicity or the ability of a metal to remove oxygen from compounds, usually organic molecules. Tailoring d-band center can control the metal oxophilicity; the closer the d-band is to the Fermi level, the more oxophilic a metal will be. With smaller coordination, more free atoms in the kinks, edges and defects tend to have to shift their d-band center closer to Fermi level in order to maintain the same occupancy of d-state electrons [18].

4

Oxophilicity tends to increase as you go up the group and to the left of the periodic

table. Left side d-block elements with low effective nuclear charge and low

electronegativity are highly oxophilic [20]. The f-block elements, also, due to their

small ionization energies of their outer electrons can easily transfer to the needs of the

highly electronegative oxygen atoms, to achieve their octet rule.

2.2. *HDO*
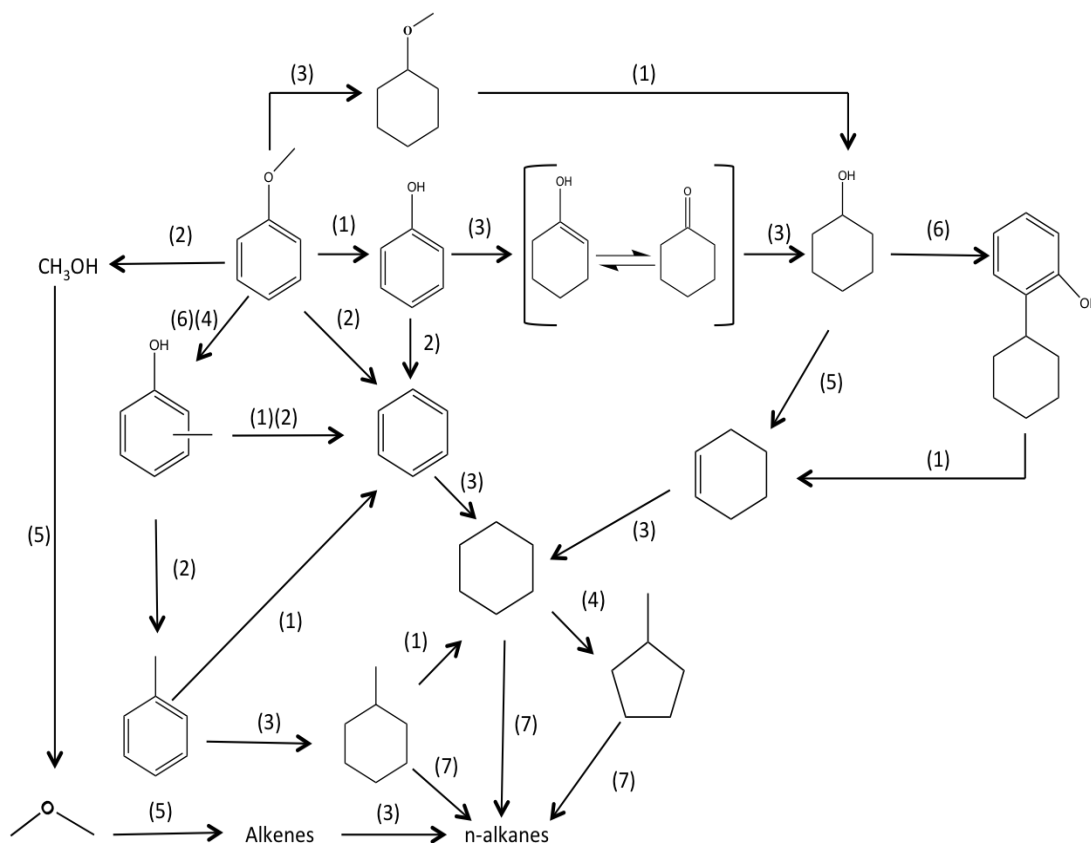
Figure 2. Reaction network of anisole (1) dealkylation and demethylation; (2) direct deoxygenation; (3) hydrogenation; (4) isomerization; (5) dehydration; (6) ring opening alkylation; and (7) ring opening reaction.   [3]

Physical processes include filtration; while chemical processes like esterification and catalytic processes like HDO. Catalytic HDO, however, is a close relative of hydrodesulfurization (HDS) and hydrodenitrogenation (HDN) both, of which are very prevalent processes in the refining industries. The content of nitrogen and sulfur in biomass is very low and we do not worry about them as much. During bio-oil upgrading, several processes and series of HDO reactions take place at relatively high temperatures (300-500°C) to remove oxygen from lignocellulose biomass.
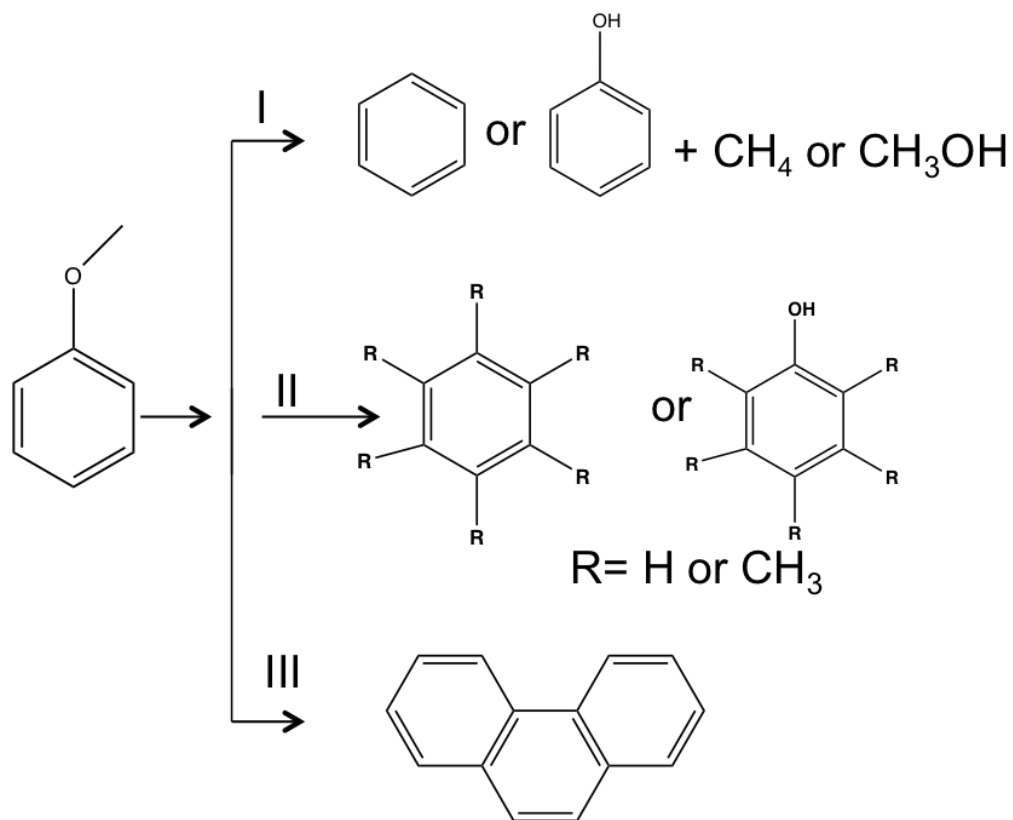
Figure 3. Scheme: conversion of anisole via (I) deoxygenation and hydrogenation (II) transalkylation. (III) Condensation reactions. Note the loss of carbon in route I. reprinted as depicted in [3].

6

These series of reactions include but not limited to deoxygenation, hydrogenation, hydrogenolysis, decarboxylation, and transalkylation can occur during this process, as seen in Fig. 2 and Fig.3 [3]. This study investigates more generally route (I): hydrogenation and deoxygenation reactions to benzene and phenol, as detailed in Fig. 4. Since Anisole belongs to ethers, with the $C_{aromatic}$—O—C_{alkyl} groups, dealkylation and demethoxylation have become of particular interest. Unlike transalkylations, as shown in Route II in Fig. 3, which preserves the carbon number, demethoxylation and dealkylation lead to reduction in carbon content, increased hydrogen consumption, and by products like coke that poison catalyst.

Nonetheless, the importance of these series of reactions in deoxygenating bio-oil cannot be ignored. Several reports have confirmed that at least 60% of compounds in lignocellulosic mass contain one or more methoxy groups[3]. Deoxygenation is important owing to the fact that phenolic products of lignin have high oxygen content. This high oxygen load results into very many undesirable properties such as high viscosity, thermal instability, corrosiveness and poor heating value [21]. In addition, there is a tendency to re-polymerize if the oxygen content is not rescued[22]. HDO is an effective pathway to upgrade these oxygen-rich bio derived fuels[23].

In Route II, as seen in Fig. 3, an example is a study by Xinli, Lobban, Resasco *et al.* which discussed bi-functional transalkylation and hydrogenation reactions[24]. Comparisons on mono-functional and bi-functional catalysts were made. With mono-functionality on HBeta zeolite, a methyl was broken off from methoxyl and transferred to the ring of anisole leading to products such as phenol, cresols, and xylenols as the

major products of anisole. While on the metal, there is less transalkylation and more cleavage, and carbon losses are seen to yield benzene and toluene. When combined, the bifunctionality led to both hydrodeoxygenation and methyl transfer taking place.

Route III is very prominent in reactions at high temperatures over 400 °C, and tends to cause severe aromatic condensation[25]. This results in polycyclic aromatic hydrocarbons (PAHs) or chars. Also reports have been made of hydrodeoxygenation of anisole in a toluene solvent have showing possible condensed aromatics.
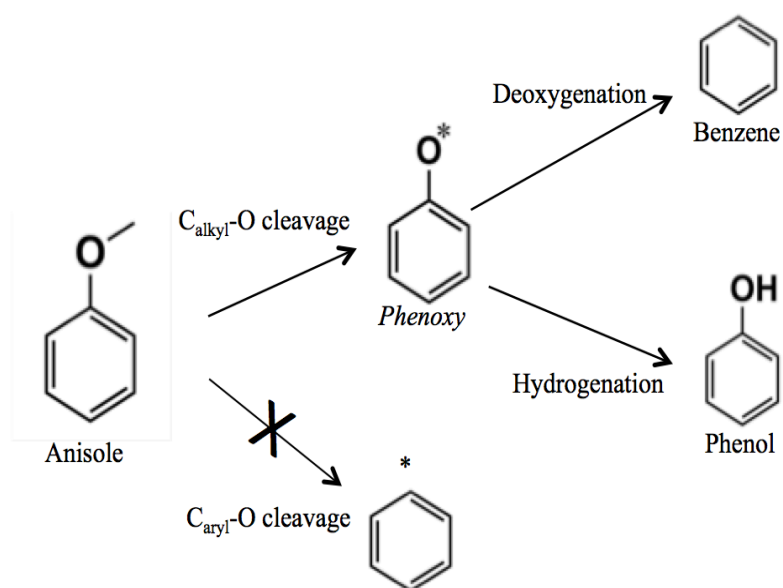
Figure 4. Pathway for HDO of Anisole, for this study.

2.3. Catalysts for HDO

The synthesis and function of numerous current technologies and products involves one or more catalyst systems. Modern life and heterogeneous catalysis have become

increasingly indispensable. Catalysts are used for over 85% of processes and products in chemical industry[26]. Particularly for bio-oil upgrading, catalyst systems that are active, selective and stable are needed now more than ever. Catalysis science, in the previous twentieth century was mostly concerned with enhancing catalytic activity especially the turnover rate, to make more product molecules per catalyst weight in a given time, rather than selectivity for the reactions. Catalysts not only improve the selectivity towards desired products, but also provide lower energy alternate routes in
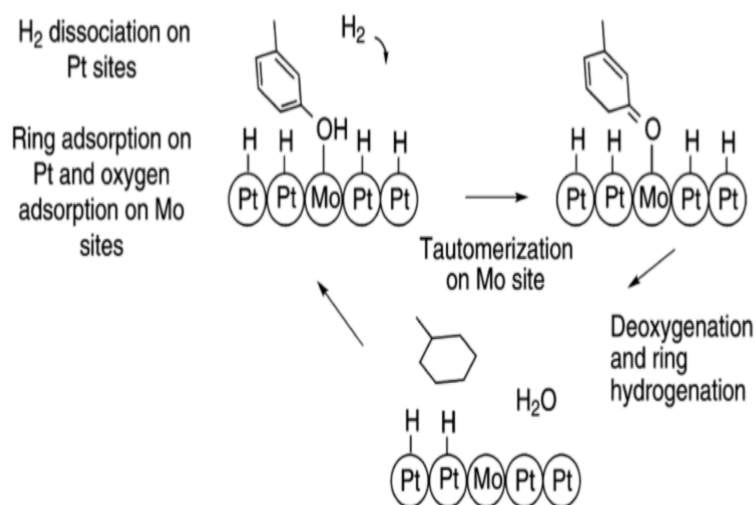
Figure 5. Schematic representation of the proposed mechanism on bi-metallic catalyst specifically for deoxygenation, showing how each metal has a disparate role [24].

reactions.

Understanding the relative strength of adsorbate-metal relationship such as carbon-metal and oxygen-metal bond strength will shed some light on several pathways that exist in biomass upgrading. We know that catalysts can work in the same phase as the reactants, thus referred to as a homogeneous catalyst, or more commonly as a

9

compound in another phase, known as a heterogeneous catalyst. The biggest cost in industry is separation, and heterogeneous catalysts come with a steadfast advantage of low separation costs. Several studies have looked at catalysts for bio-oil upgrading and a few are discussed such as metal-metal bi-functional catalysts[27].The argument for bi-functional catalyst is that one catalyst is rarely able to perform the numerous reaction steps that are always bound to happen in a lot of catalytic reactions, especially for the biomass upgrading. Bi-functional catalysts contain active sites such acid sites and metal sites that catalyze complementary or successive reaction steps in tandem, as shown in Fig. 5. Common example includes Pt that is modified by adding 3d transition metals such as Ni, Fe and Ti. Kitchin et reported that the Pt surface d-band was broadened and lowered in energy by interactions with the subsurface $3d$ metals, resulting in weaker dissociative adsorption energies of hydrogen and oxygen on these surfaces [28, 29].

On supported metal catalysts such as Pt/SiO2, hydrodeoxygenation of anisole seems to predominantly yield phenol at low space-time, but as W/F increases, the yield to benzene increases at the expense of phenol. Over aluminosilicate-supported Ru and Ni catalyst, similar results are found[30]. Therefore, HDO catalysts can significantly affect the selectivity and reaction pathways.

2.3.1. Particle Size Studies

The rate and product distribution of chemical reactions catalyzed by metals can depend on the particle size of supported catalysts. The variations in energies of interactions

between chemisorbed species and surface sites of different configurations in the metal

associated with terraces, steps, and kinks are a possible justification for this

phenomenon. Gabor *et al.* classifies three types: structure-sensitive reactions, structure-

insensitive reactions, and reactions that show both behaviors, depending on the

experimental conditions[2]. The relative concentrations of terraces, steps, and kinks do
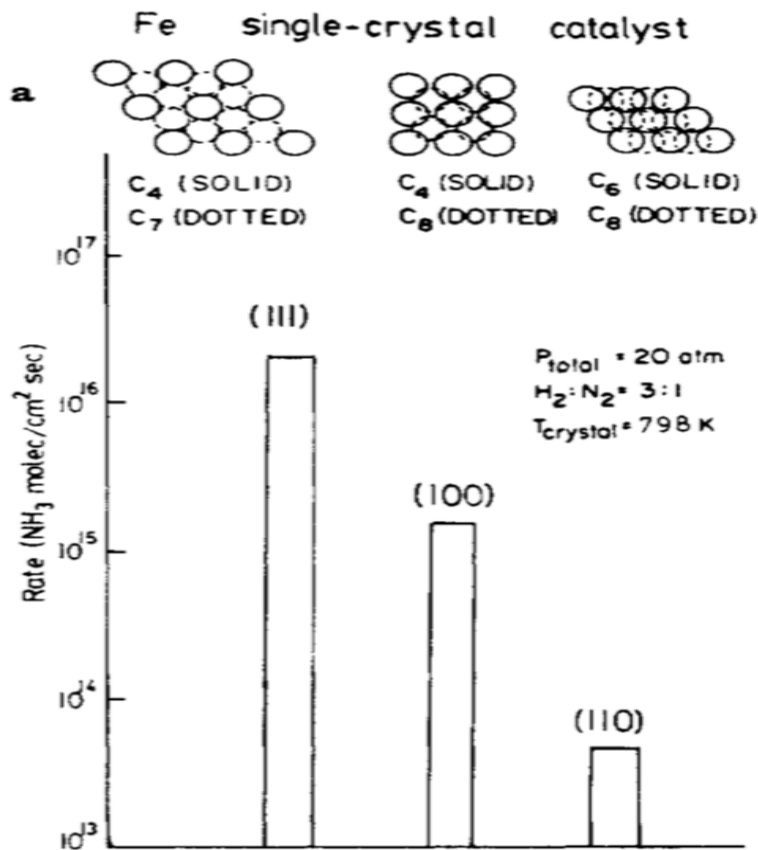
Figure 6. Structural sensitivity in the ammonia synthesis over Fe surfaces [2].
vary with catalyst particle size; it is therefore reasonable to question how changes in

local atomic structures and surface defects will alter reactions.

The greatest structure sensitivity has so far been studied in ammonia synthesis from hydrogen and nitrogen over iron and rhenium as shown in Fig. 6. Reaction rates varying in several orders of magnitude were observed, amongst the different surface configurations for similar metals. The catalytic activity was higher on the more open, edged and rough surfaces [31]. Therefore, the roughness of surface and openness of the surface atoms can be related to the catalytic activity for ammonia synthesis and many other reactions. The study found that the closest packed surface of Fe(110) has the least activity and the most open structure Fe(111) has the most activity.

Structure sensitivity and the effect of particle size are concepts of utmost importance and they give an insight into designing new selective catalyst systems for biomass upgrading. Selectivity towards specific products is of key interest, and in this case, the selectivity towards benzene or phenol from anisole. Selective processes do not only offer cleaner chemistry and better environmental protection, but also allow for improving the use of resources thus leading to more economic production[32].
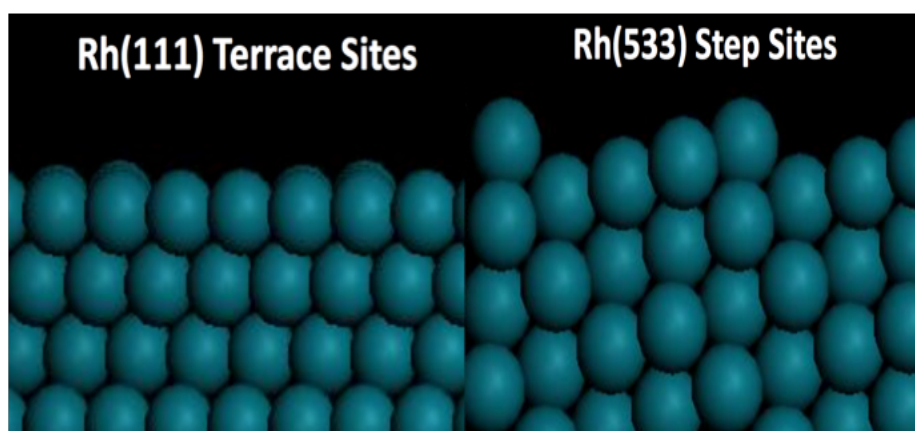
Figure 7. Side view comparison of a close-packed Rh(111) and Rh(533) step site with one Rh atom high step in the (100) plane, and 4

Most recently, Nhung *et al.* have evaluated the effect of particle size on hydrodeoxygenation of m-cresol on rhodium [18]. Direct cleavage of the —OH bond of m-cresol was found to be favored on smaller particles of the catalyst, modeled by Rh(533). Their choice of the metal rhodium was due to its centrality in d-band center between Pt(111) and Ru(0001) that had earlier been studied. However, the reactivity of the stepped site also came with a downside of deactivation with barrier to clean the surface exceedingly high. For example, the energy requirement to clean off —OH* to form H_2O was 127 kJ/mol on the steps compared to 68 kJ/mol on the terrace surface.

2.4. First-principle Modeling

An important question now that that arises is how experimental studies for particle size will be modeled by first-principles DFT calculations. Models based on first principles have come in a prime time of catalytic function and discovery of materials. Advancements in biomass research have necessitated detailed understanding electronic interactions, and bonding on metal catalyst surfaces during aromatic conversions. It is well known that discovering and improving catalysts is a challenging process. Density functional theory calculations can reveal the sites, which the molecules of interest bind to most strongly. With this in mind, proper placement of molecules is ensured during the calculations of adsorbate-substrate interactions.
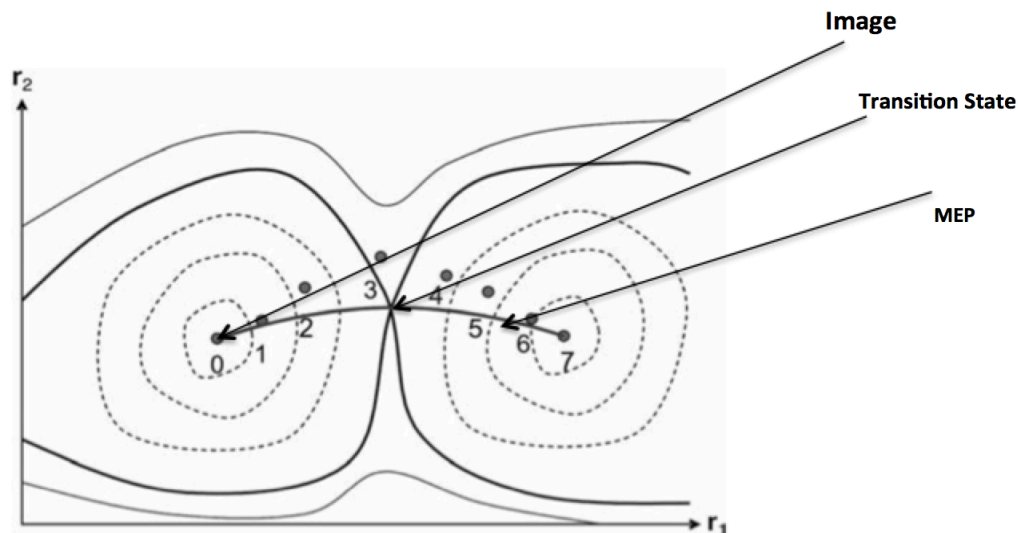
Figure 8. NEB follows a minimum energy path from local minima (reactant) to another local minima (product), via a saddle point, to estimate transition states.

As an example, if the adsorption energy of a molecule shows the most stability on a bridge site, other sites can be ignored to save computational cost and optimization time. Note that the most stable molecular adsorption configuration may not be the most active configuration, however, calculations using the most stable configurations still provide valuable information for the reaction mechanism.

Otherwise, while building a reaction path using NEB, one or more maxima may be observed due to the fact that the molecule was not originally in its most stable site, and had to diffuse to the stable site first resulting in presence of stable intermediate configurations. Henkelman *et al.* define a path connecting the initial and final states that typically has the greatest statistical weight, as Minimum Energy Path (MEP)[9, 33]. The MEP is found by constructing a set of images with graphical user software

such as VNL (virtual Nano Lab), typically on the order of 4–20 images, between the known minima of initial and final states [9, 33]. By adding a spring interaction, this ensures that adjacent images are equidistant; this constrains the optimization of the images, acting similar to an elastic band. Climbing NEB is used sparingly in case of two or more structures that are very close to the saddle point in energy. Otherwise, refined NEB can be run with images close to the highest point as new initial and final states. Therefore, it is generally important to study appropriate sites for simulations to avoid multiple saddle points due to surface diffusions and lateral interactions during theoretical surface reactions.

Rhodium, which up to temperatures of its melting point at 2236 K, is an FCC metal [34]. The (111) surface configuration of FCC metals is an idealized model due to its high symmetry. FCC(111) results from cutting fcc metals such that the surface plane intersects x, y and z planes at the same value and this leaves a 3-fold symmetry. As shown in the Fig. 9 below, all atoms are noted to be highly coordinated, very smooth and offer variety of adsorption geometries such as bridge, on-top sites, and hollow sites between three carbon atoms. With DFT calculations, several atoms can be placed in all of these sites and evaluated for stability on an fcc surface.
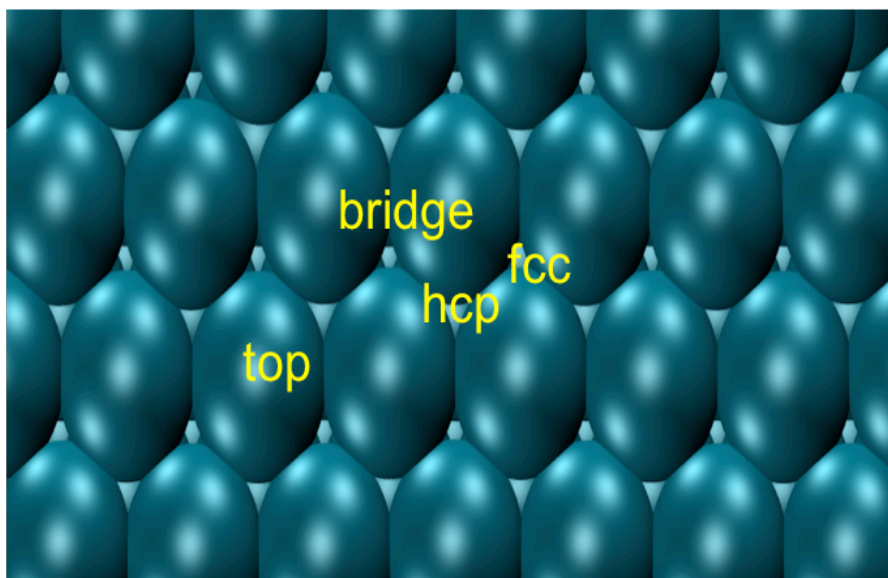
Figure 9. Bird's eye-view of an FCC(111) surface.

2.5. Adsorption of atoms and molecules on the metal surface

Contributions to the adsorption of molecules and atoms on metal surfaces of interest can be either chemical or physical in nature. Chemical binding typically implies either an ionic interaction, by transfer of charges between substrate and adsorbate, or a covalent interaction, where orbitals deriving from the adsorbate and the substrate form new bonding and anti-bonding linear combinations[35]. Interactions by induced

16

molecular dipoles, and instantaneous dipoles in adsorbate molecules are possible, and

this gives rise to van der Waals interactions (vdW). As discussed in methods, vdW

corrections will be used to account for possibilities of van der Waals interaction.
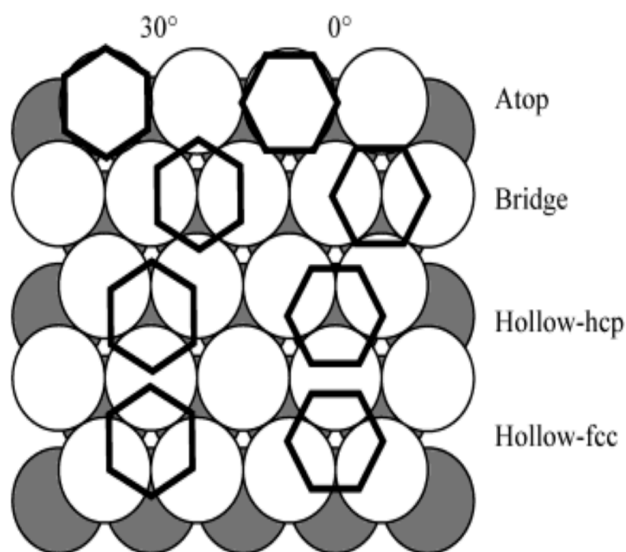
Figure 10. Schematic of high-symmetry adsorption sites on monocyclic
aromatic rings [41].

As shown in Fig. 9, adsorption of small atoms like hydrogen, carbon and oxygen is

relatively easy to evaluate over an fcc(111) surface on atop, hollow, and bridge.

Hoflund defines the "bridge" as the bond midpoint site that is above the center of a

bond formed between two surface metal atoms. The "hcp" hollow as an eclipsed site

which is directly over a second- layer metal surface atom, and the fcc site is over the

center of a triangle formed by three close packed surface metal atoms[36].

Particularly for hydrogenation, hydrogen atom as one of the simplest adsorbates, lots of

studies have been done[36-38]. Norskov *et al.* have studied hydrogen chemisorption

energies for a number of metals using DFT calculations with the adsorbate at the fcc

site [37]. The result was a "volcano plot" with transition metals showing correlations between catalyst activity and adsorption free energies.

Larger molecules, such as anisole, on the other hand present numerous adsorption geometries ranging from bridge (30), bridge (0), atop (30), atop (0), hollow (30), hollow fcc (30), and tilted di-σ [39].

As shown in Fig. 11, the adsorption of rings such as anisole, benzene, phenol can be assigned as di-σ and π-bonding. Di-σ bonding is stronger compared to π-bonding on the metal substrate. This configuration leads to minimal distortion the from gas-phase geometry. Anisole binds primarily through a combination of π-orbitals with d-orbitals of metal.
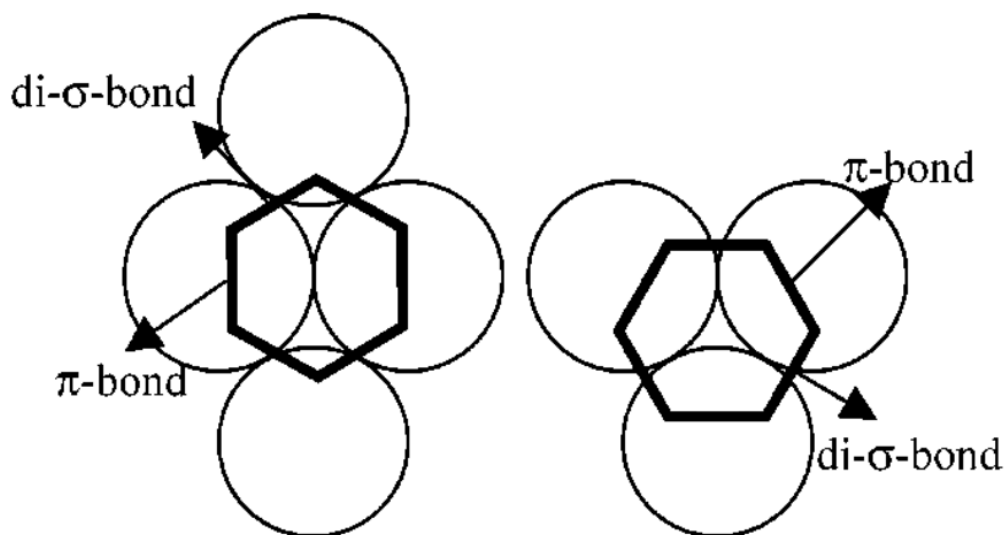
Figure 11. Illustration of the π- and di-σ bonds of aromatic ring at the bridge and hollow site [39].

Numerous studies have been carried out for adsorption on metal (111) surfaces. Anisole is a mono-substituted aromatic compound; its adsorption geometries can be closely related to benzene on a metal surface. However, this is not the same for other polycyclic aromatic compounds since steric interactions lead to complications in adsorption orientations. The more the bridges (bonds connecting two Rh) atoms, the more the configuration is preferred. The axial overlap in sigma bonds renders them more strength than pi bonds that otherwise results from lateral overlap of p-orbitals.

Chapter 3: Theoretical Methods

The periodic plane-wave density functional theory was used to for calculations. These DFT methods are incorporated in the Vienna *ab initio* Simulation Package (VASP) [40, 41]. The generalized gradient approximation (GGA) functional, introduced by Perdew, Burke, and Ernzerhof (PBE), was used to calculate the electron exchange-correlation energy, E_{xc} of interacting electrons[42]. Using the DFT-D3 method, vdW corrections are calculated[43]. All simulations such as for potential energy, interatomic forces, atomic and lattice relaxations, molecular dynamics, and vibrational analysis for transition state analyses were all corrected for van der Waal interactions.

The 4×4 close packed Rh(111) and Rh(533) surfaces are modeled with a lattice constant of 3.81 Å, close to reported values of 3.803 Å [34]. A 4×4 unit cell was chosen to minimize lateral interaction between neighboring benzene molecules. Repeated slabs of Rh (533) and Rh (111) were then built. Both slabs consist of 80 Rh atoms and were modeled with four layers with vacuum space of 15 Å of vacuum

separating the slabs in the z-direction chosen to insulate successive layers. All of reactants, intermediates and products structures were optimized until the forces on each atom were below 0.01 eV/Å. The top two layers were allowed to fully relax in all calculations, whereas the bottom two layers were fixed to the bulk distance of the metal.

Adsorption studies were carried out first for example; for example the adsorption of anisole on a rhodium metal surface was defined as:

$$E_{ads} = E_{TOT}(Anisole + surface) - E_{TOT}(Anisole) - E_{TOT}(surface) \qquad (1)$$

where E_{TOT} (anisole+Rh surface) is the DFT calculated total energy of anisole bound on the metal surface. $E_{TOT}(Anisole)$ defines the total energy of an isolated phenol molecule, $E_{(surface)}$ is the total energy of the bare slab.

The adsorption was analyzed at strategic adsorption sites discussed above such as: fcc and hcp (threefold sites), bridge (twofold site) and atop (single-fold site) on the metal surface. Spin polarized calculations were performed for the atomic O and H atoms in the gas phase.

Transition states were obtained by building reaction trajectories using the Nudge Elastic Band (NEB) method [9, 44, 45]. As discussed before, the minimum energy path (MEP) is built between an initial and final DFT calculated states. First, the geometry of the reactant is optimized followed by geometry optimization of the product, and then an optimization of the MEP. The same computational parameters are used such as unit

cell and cut off energy. In cases where convergence was not achieved, optimization is restarted using the last optimization VASP output files.

Chapter 4: Results and discussion

This section consists of three parts. First, the computed adsorption geometries at different high symmetry sites on rhodium are discussed. Second, elementary steps of reactions at the rhodium surfaces are presented including successive hydrogenation, demethylation, and demethoxylation. Lastly, results about the fate of the phenoxy intermediate are presented.

4.1. *Adsorption and geometries of anisole on Rh(111) and Rh(533)*

Here, detailed results are reported for the adsorption energies, the stabilities of various adsorption geometries, and the adsorption-induced changes after surface relaxations.
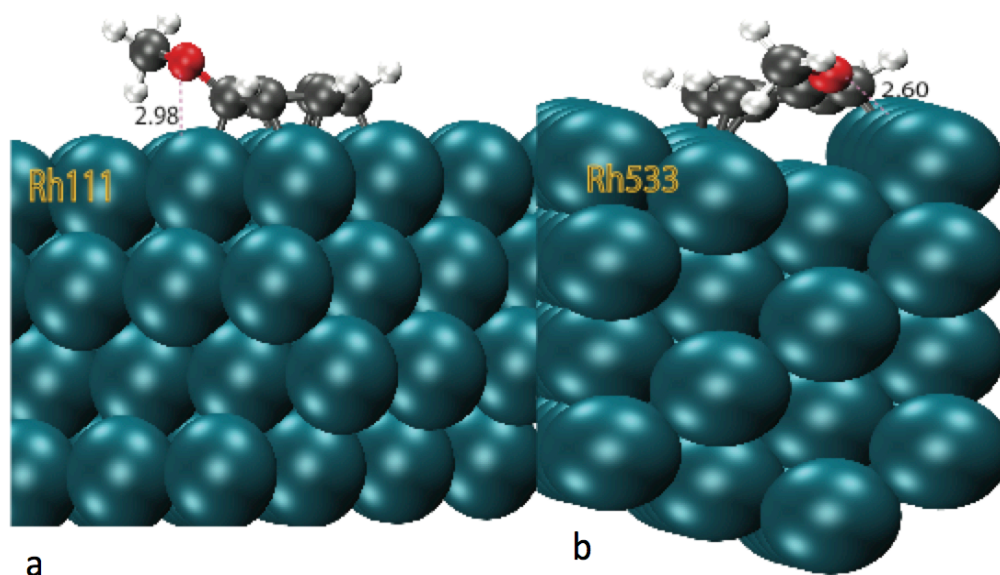
Figure 12. Side view of the Rh—O bond and length on (a) terrace and (b) step configurations.

Foremost, the energies of different adsorption configurations of the anisole molecule over Rh(111) and Rh(533) surfaces were calculated and compared as shown in Table 1 and Table 2, respectively.

Table 1. High symmetry adsorption energies of anisole on Rh(111) at low coverage, in kJ/mol

Mode	E_{ads}
Bridge 30	-283
Hollow hcp	-277
Hollow fcc	-275

From this study, adsorption of anisole on surfaces of Rh(111) was found to favorably adsorb and stable on a "bridge 30" configuration, and closely followed by the hcp hollow site.
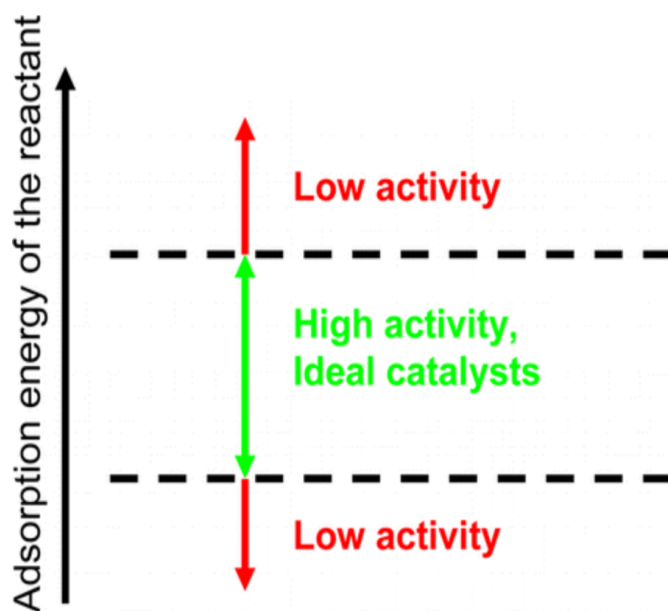
Figure 13. Illustration of the Sabatier principle[1].

Anisole prefers to lay flat on the surface with the six-carbon atom ring shared amongst four rhodium surface atoms. The methoxy group(C—OCH3) is tilted by 22° angle from the surface as shown in Fig. 12(a). C—H bonds make an angle of 19° with the surface. As discussed before, the more the bridges (C—C bonds spanning over two Rh atoms), the more the configuration is preferred because of favorable overlap between Rh d-orbitals and C p-orbitals. The adsorption energy of anisole is -283 kJ/mol, which for comparison is more than that reported for Pt(111) of -225 kJ/mol and but lower than that on Ru(0001) of -263 kJ/mol[10]. We postulate that fcc Pt(111), fcc Rh(111) and hcp Ru(0001) are more closely packed surfaces than Fe(110), and C's in anisole

form more bonds with metal atoms. Additionally, the *Sabatier principle*, illustrated in Fig.13 which states that the adsorption of the reactants on the catalyst surface should be neither too strong nor too weak to achieve high activity[1]. In other words, the interaction of catalyst surface and adsorption should be *just right*.

In this comparative study, Fe(110) seems to just be right at -232kJ/mol. We anticipate that at higher coverage, anisole will slide off into the hollow site due to repulsive interactions between adsorbed anisoles. Additionally, research has shown that hollow can provide a more compact way of adsorption at higher converges[39].

The adsorption energy of anisole on Rh(533) is trickier due to the presence of step, and also the additional —OCH$_3$ group on anisole. Where do we place the adsorbates on Rh(533)? Questions arise whether to place the adsorbate on the step, terrace, and a mixture of both? —OCH$_3$ group is inert and will experience repulsions, as it gets closer to the Rhodium atoms

Table 2. Adsorption energies of anisole on Rh(533) stepped surface

Mode	E_{ads}
Parallel*, O-step	-278
Perpendicular*, O-step	-259
Terrace	-277
O-Away from step	-244

* Described relative to step

Throughout these simulations, anisole is placed on various locations both on steps and terrace, and at the surface. Table 2 shows the various locations on which anisole were placed. In all sites, anisole tends to shift with the oxygen towards away from the rhodium atoms on the step. However, oxygen atom is still closer to the step atom than on Rh(111), a configuration that will later favor deoxygenation. In fact, the end goal of HDO is get oxygen as close to the metal surface so that it can be cleaved.
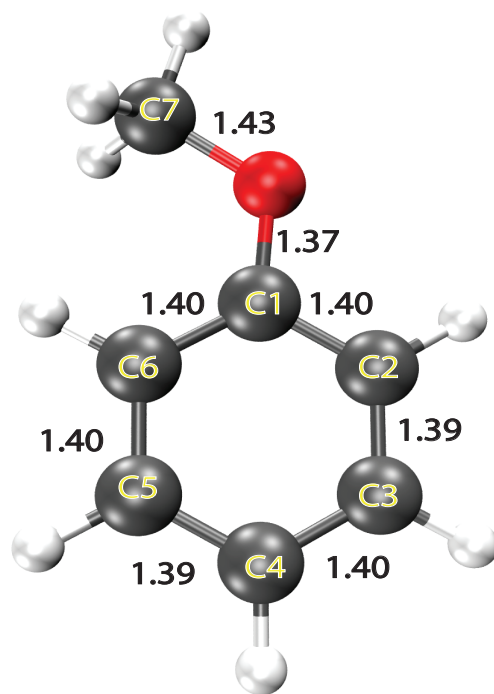
Figure 14. Gas phase neutral anisole.

With the right adsorption mode, Rh(533) seems to not have any problems with proximity of oxygen (—O—) to the surface. In fact, the sequential hydrogenation, and ultimately —cleavage of CH_x steps seek to achieve that. From this analysis, it can be concluded that the most favorable adsorption mode on Rh(533) is anisole placed

slightly parallel to the step with O —Rh bond length at 2.60 Å as shown in Fig. 12.

Comparison with Rh(111) shows that oxygen is much father away from Rh atoms at a

distance of 2.98 Å. Previous studies have shown that though "atop" sites are

unfavorable, they can be favored in defected surfaces[39]. Notice that anisole

adsorption on Rh(533) is less than Rh(111) because of two possible reasons: one being

that the step leads to less carbons attaching to the surface than on the terrace surface,

and oxygen proximity to the step does not make up for the loss of about three C—Rh

bonds, as seen in Fig. 12. Also, previous studies on phenol support this explanation,

showing that it adsorbs favorably on terrace Rh(111) than step surfaces (Rh 211)

because of inertness of the —OH group that gets repelled by the step[46].
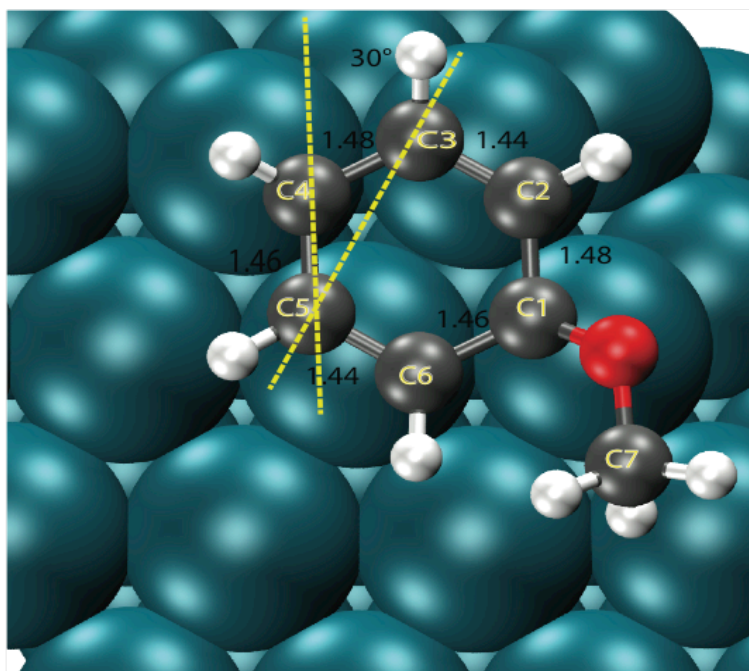
Figure 15. Bond length of anisole upon adsorption with a bridge 30 configuration

Neutral gas phase anisole has calculated average of C—C bond length of 1.39 Å and a

$C_{aromatic}$—O bond length of 1.37 Å as well as a C—H length of 1.10 Å, as shown in

Fig. 14. These values agree with recent experiments of C—C of 1.39 Å and C—H of

1.08 Å[47].

Upon adsorption on "bridge (30)" site as shown in Fig. 15, C—C bond length

significantly increases to 1.46 Å indicating substantial filling of anti-bonding pi

orbitals [33]. Aromatic adsorption on transition metals occurs mostly through π

electrons. However, it is important to note that these sites may change at higher

coverage.
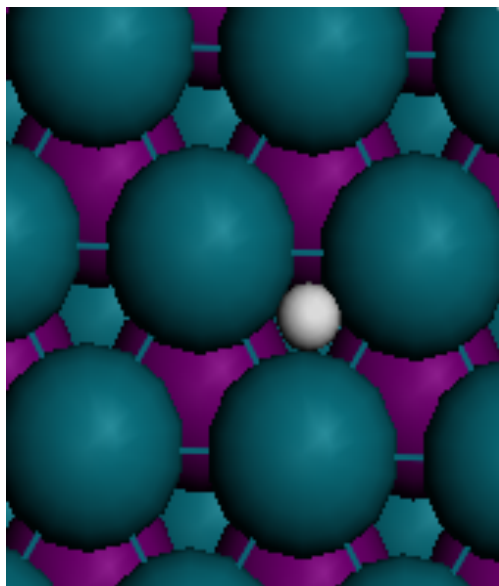
Figure 16. High symmetry site for hydrogen on Rh(111)

 For comparison, single C—C bonds in ethane is 1.50 Å. This increase of about 2 to

5% signifies that four of the C—C bonds in anisole (C1-C2, C3-C4, C4-C5, C6-C1),

upon adsorption, are becoming closely similar in strength and length to σ- bonds in an

alkane such as ethane. While two bonds, are still C = C bonds of length equals or is smaller than 1.44 Å. As already discussed in the di-σ bond and π-bond concept, four di-σ and two π-type interactions can be assigned to the bridge (30) site adsorption as seen in Fig. 11.

For the hydrogen atom, the site preference has its origin in a maximum gain of covalent bonding energy resulting from the overlap of the hydrogen s and the metal empty d-orbitals and from a minimal Pauli repulsion. Hydrogen prefers to adsorb on a hollow fcc site with potential bonding to three rhodium atoms as seen in Table 3 and Fig. 16. This is in agreement with investigations on Pd(111) for hydrogen adsorption where the fcc site was found to be about 50 meV more stable than the hcp site[48, 49]. However, atomic hydrogen is highly mobile and will likely just diffuse to various locations that are within a -5 kJ/mol difference in adsorption.

During deoxygenation reactions, when the oxygen is cleaved off the aromatic ring, and it was placed at the fcc site, which is the preferred adsorption site at -596 kJ/mol on Rh(111) and -656 kJ/mol on Rh(533), respectively. As a measure of oxophilicity, this adsorption energy of atomic oxygen was used as a descriptor in previous studies[16].

Table 3. Hydrogen adsorption energies on Rh(111) terrace surface.

Mode	E_{ads}
Hollow fcc	-55
hollow hcp	-54
Atop	-40

Q. Tan *et al.* calculated atomic oxygen on Pt(111), Ru(0001), and Fe(110) and reported -481, -650 and -698 kJ/mol respectively, indicating that the order of metal oxophilicity is Pt(111) < Ru(0001) < Fe(110). Noticeably, Rh(111) lies just above Pt(111), and Rh(553) lies between Ru(0001) and Fe(110). Studies by Lopez-Moreno *et al.* have shown atomic oxygen prefers to adsorb on fcc and hcp three fold hollow sites with slight preference for fcc(111) surfaces [50].

Table 4. Adsorption energies (kJ/mol) of reactant, products and intermediates in the hydrodeoxygenation of anisole on Rh(111) and Rh(533) surfaces.

	Rh(111)	Rh(533)
Anisole	-283	-278
Phenol	-225	-240
Benzene	-218	-232
H	-55	-64
O	-596	-656
C	-715	-792

4.2. Reactions

Here we show energy diagrams, and images of several elementary steps and their corresponding structures. Reactions considered here include demethoxylation, demethylation, and dehydrogenation of anisole, and ultimately deoxygenation and hydrogenation of phenoxy intermediate.
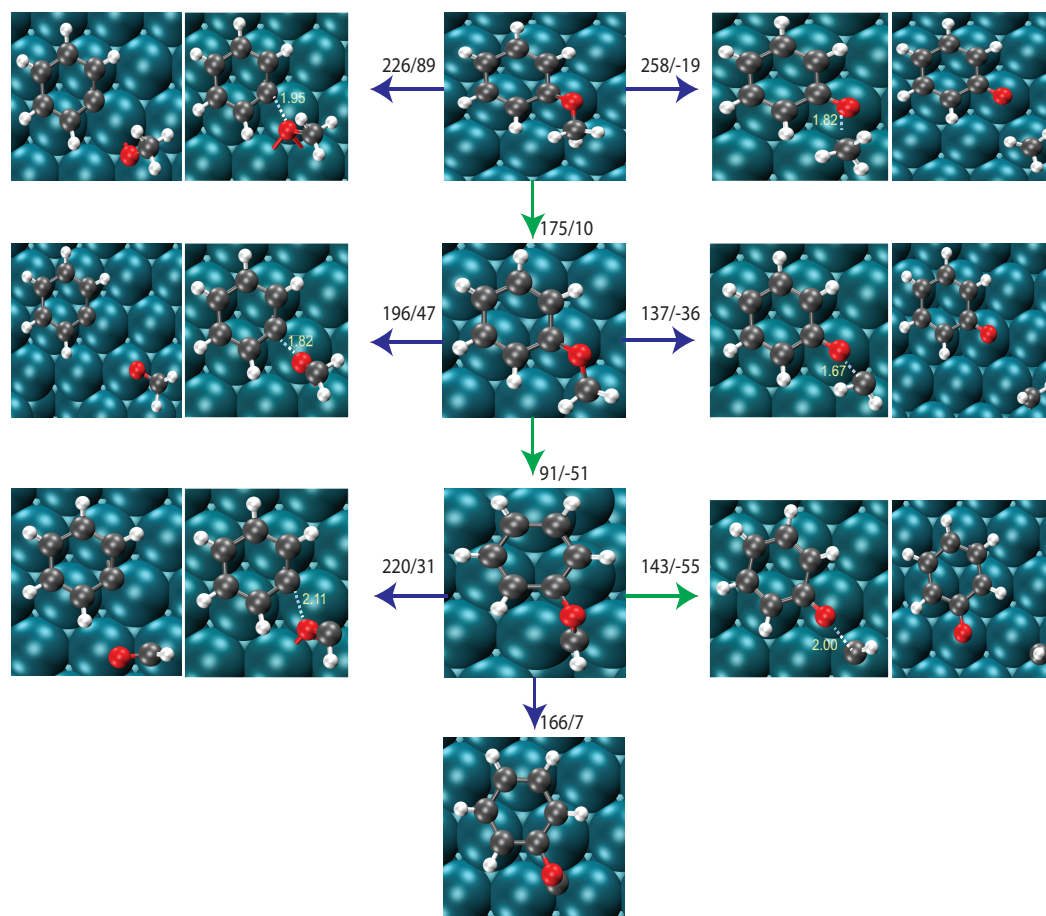
Figure 17. Layout of DFT calculated reactant, transition state and product structures for $C_{aromatic}$—O bond breaking, C_{alky}—O and dehydrogenation reactions of different Ph—O—CH$_x$ (1≤x ≤3) on stepped Rh(111) surface

One proposed pathway is to directly cleave the methyl (—CH$_3$) over Rh(111). In this case, Rh—CH$_3$ distance would need to reduce from 3.01 Å to a Rh—CH$_3$ distance of 2.06 Å in the transition state. Additionally, C_{alkyl}—O increases from 1.43 Å to 1.82 Å in transition state so it can be broken forming a phenoxy intermediate, which in turn would be hydrogenated to form a phenol or deoxygenated to phenyl intermediate. This pathway turns out to thermodynamically favorable with reaction energy of -19 kJ/mol

but it remains kinetically unfavorable with an activation barrier of 258 kJ/mol.

The $C_{aromatic}$—O bond may also be directly cleaved to form a phenyl intermediate, which could then be hydrogenated to benzene. In order to cleave —OCH_3 from anisole on Rh(111), the $C_{aromatic}$—O bond increases from 1.37 Å in the reactant to 1.93 Å in the transition state. Additionally, the O—Rh would need to dramatically drop in distance to be closer to the Rh surface from 2.9 Å to 2.04 Å in the transition state. The resulting activation barrier for these two bond adjustments is very high at 226 kJ/mol. It is also highly endothermic at 89 kJ/mol.

Previous studies have discussed the possibility of dehydrogenating sequentially of the —CH_3 moiety. As shown in Fig. 17, the first –H removal is more favorable to remove at 175 kJ/mol than both demethylation and demethoxylation discussed above. At this point, the Ph—O—CH_2* can be cleaved at the C_{alkyl}—O or the $C_{aromatic}$—O, however, a second hydrogen can also be removed at a much less energy barrier of 91 kJ/mol compared to 137 and 196 kJ/mol for other pathways. This successive dehydrogenation is both kinetically and thermodynamically favorable.

How about removing the 3rd H-atom? As seen from the reaction scheme in Fig. 17, removing the 3rd H-atom would create a carbon that needs to bind three rhodium atoms. It would in turn have to shift the whole molecule to accommodate for this highly reactive product. This third dehydrogenation is significantly more difficult with an activation barrier of 166 kJ/mol on Rh(111).
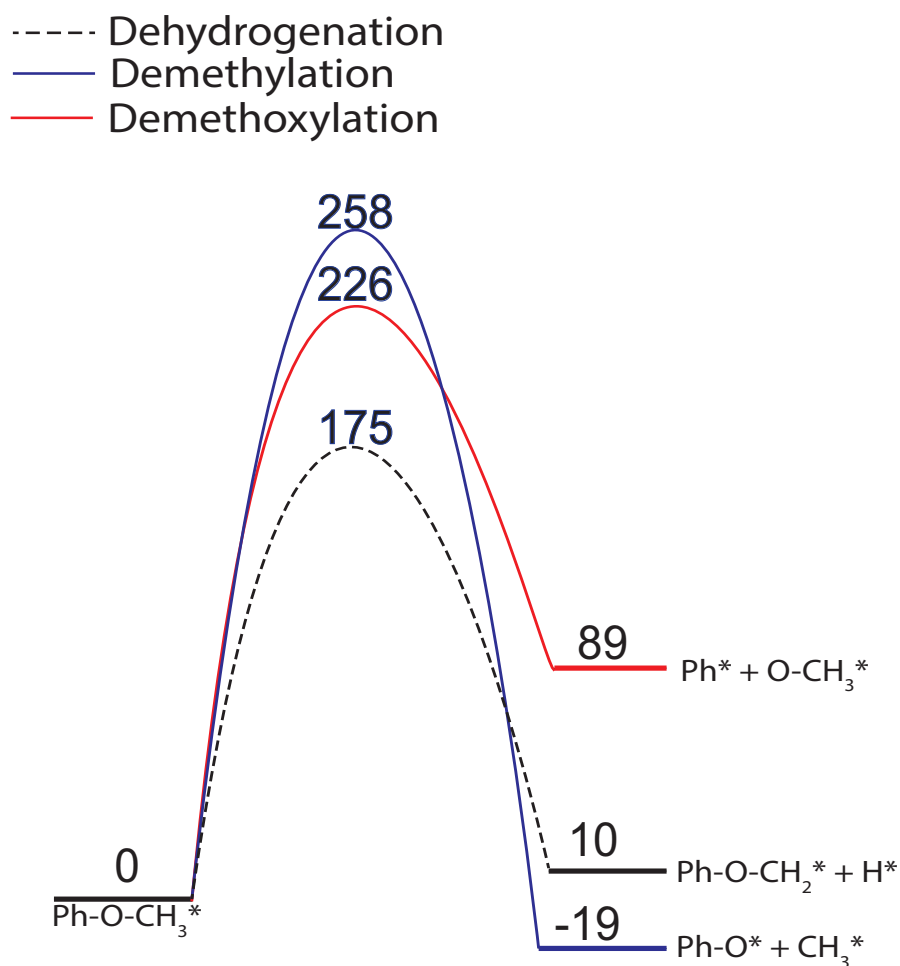

Figure 18. Energy diagram for first possible pathways for hydrodeoxygenation of anisole on Rh(111). This graph only considers the first step of demethylation, demethoxylation and dehydrogenation of Ph—O—CH$_3$

Instead, the Ph—O—CH* can now be cleaved at the C_{alkyl}—O bond, which forms a thermodynamically stable product with reaction energy of -55 kJ/mol through a lower barrier of 143 kJ/mol. Successive dehydrogenation of the —CH_x on Rh(111) has reduced the energy requirement to form a phenoxy intermediate by almost 50%. In comparison to previous studies, this pathway is that on Pt(111) and Ru(0001), reported by Q. Tan *et al*. Also, demethoxylation is almost always unfavorable in both previous studies and our current simulations.

4.2.2. Reaction paths for HDO of anisole over Rh(533)

The stepped surface Rh(533) did exhibit similar pathways as the more oxophillic metals previously studied, i.e. Ru(0001) and Fe(110). There are some subtle differences that will now be discussed. In terms of oxophilicity, oxygen adsorption is the main descriptor. Rh(533) surface has been shown to have a high affinity for oxygen atoms than Rh(111), Pt(111) and slightly more than Ru(0001). In some reactions, it behaves closely like Ru(0001) while in other reactions, it behaves like Fe(110). Fig. 19 summarizes the various first possible pathways that were observed for Rh(533). Notice that the thermodynamics may not always follow the kinetics, as we observe from Fig. 19 that while —CH_3 direct cleavage is the most exothermic, it has the highest activation barrier. A possible explanation is that the products formed such as phenyl*, phenoxy, and methyls (CH_3*) are thermodynamically stable product on the Rh surface. Hence, the Bell-Evans-Polanyi Principle does not hold in this case, especially for radicals and reactive intermediates.

Similar to the investigations done on for Rh(111), the $C_{aromatic}$—O bond on Rh(533) stretched from 1.42 Å to 1.70 Å in the transition state with an energy barrier of 141 kJ/mol. This is a relatively lower barrier compared to 226 kJ/mol for the terrace surface. It is also lower than the values reported on Pt(111) but more than Ru(0001) and Fe(110). Upon cleavage, the —OCH₃ binds atop of one rhodium atom to form a Rh—O bond with length of 2.15 Å.
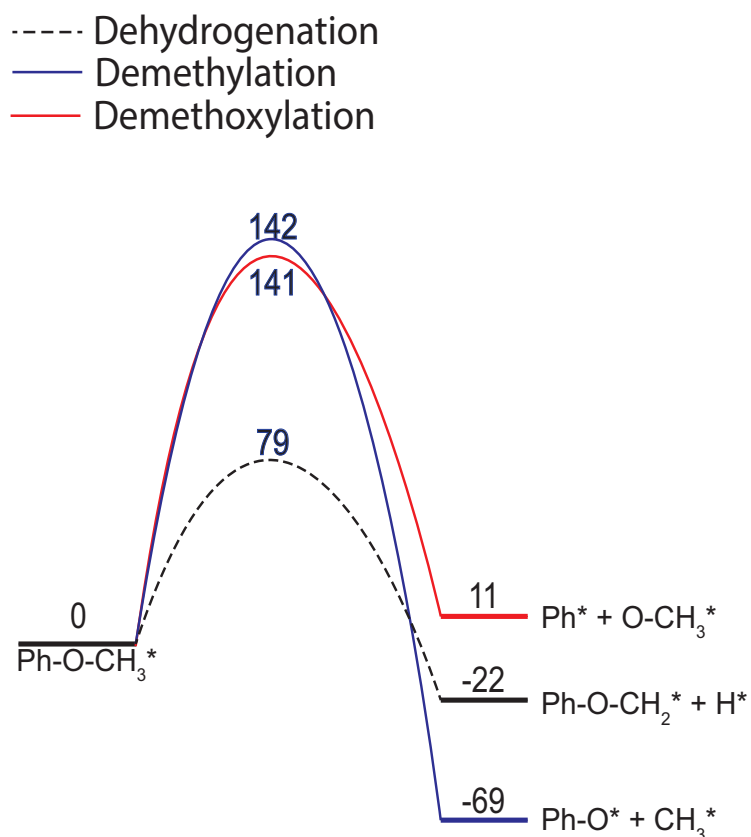
Figure 19. Energy diagram for first possible pathways for hydrodeoxygenation of anisole on Rh(533). This graph only considers the first step of demethylation, demethoxylation and dehydrogenation of Ph—O—CH₃

The barrier for demethoxylation and demethylation is within 1 kJ/mol difference. Both

values are half as high as those calculated for Rh(111). Recall that the bond length of

O—Rh of anisole adsorbed on rhodium was 2.6 Å on Rh(533) compared to 2.98 Å on

Rh(111). This proximity of oxygen to the rhodium atom on a stepped surface compared

to the terraced surface is one of explanation for the reduced energy barrier to
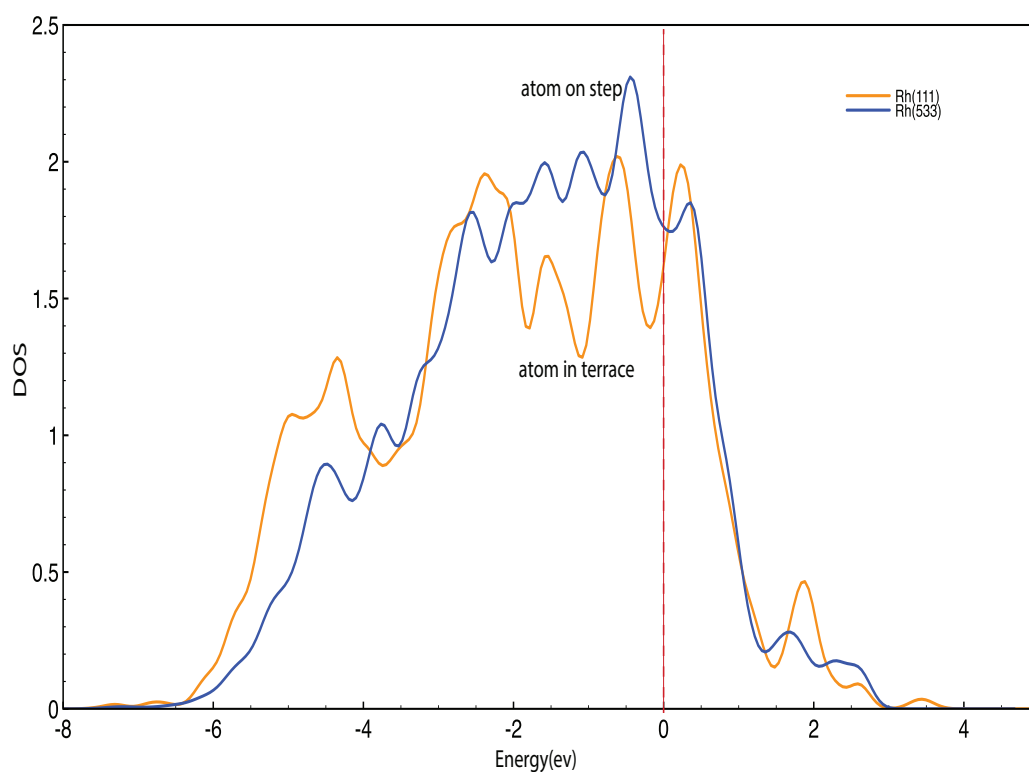
Figure 20. Density of states for an atom from rhodium at the step on Rh(533) and from terrace on Rh(111). d-band center calculated as: -1.8 ev for Rh(111) and -1.5 ev for Rh(533)

demethylate and demethoxylate. This is, in addition, to the high oxophilicity due to the

shift and narrowing of the d-band center caused by low coordination in steps, edges

and kinks.

As shown in Fig. 20, for increasingly less coordinated atoms on surface, bulk or

adatoms ,such as Rh(533), the density of states become narrower and sharper and shift

towards the Fermi level. The shift moves the antibonding states formed by

hybridization of anisole and rhodium above the Fermi level, and as the number of

empty antibonding states increase, bonds become stronger. Step atoms on Rh(533) will

be able to cleave C—O bond due to the stronger Rh—O bond interaction.

Experimentally, this translates to smaller particle sizes of catalyst that are more likely

to have irregular, defected surfaces and edges.

However as shown in Fig. 19, the removal of one H-atom from —CH$_x$ remains a

promising pathway with a barrier 50% less than the two previous pathways. With an

energy barrier of 79 kJ/mol, Rh(533) catalyzes the successive dehydrogenation of

anisole to remove just one H-atom. Unlike, on Rh(111), the reactivity of Rh(533)

makes it possible to cleave the —CH$_2$* just only after one hydrogenation step(-H), as

shown by green arrows in Fig. 21 to form a crucial intermediate, *surface phenoxy*.

The significance of less dehydrogenation steps shown by green arrows, in Fig. 17 and

Fig. 21 emphasizes the reactivity trends of Rh(111) and Rh(533). Although —CH$_3$

could not be cleaved directly on Rh(533), —CH$_2$* can be cleaved to form a surface

phenoxy without the need for an extra dehydrogenation step as it is the case for

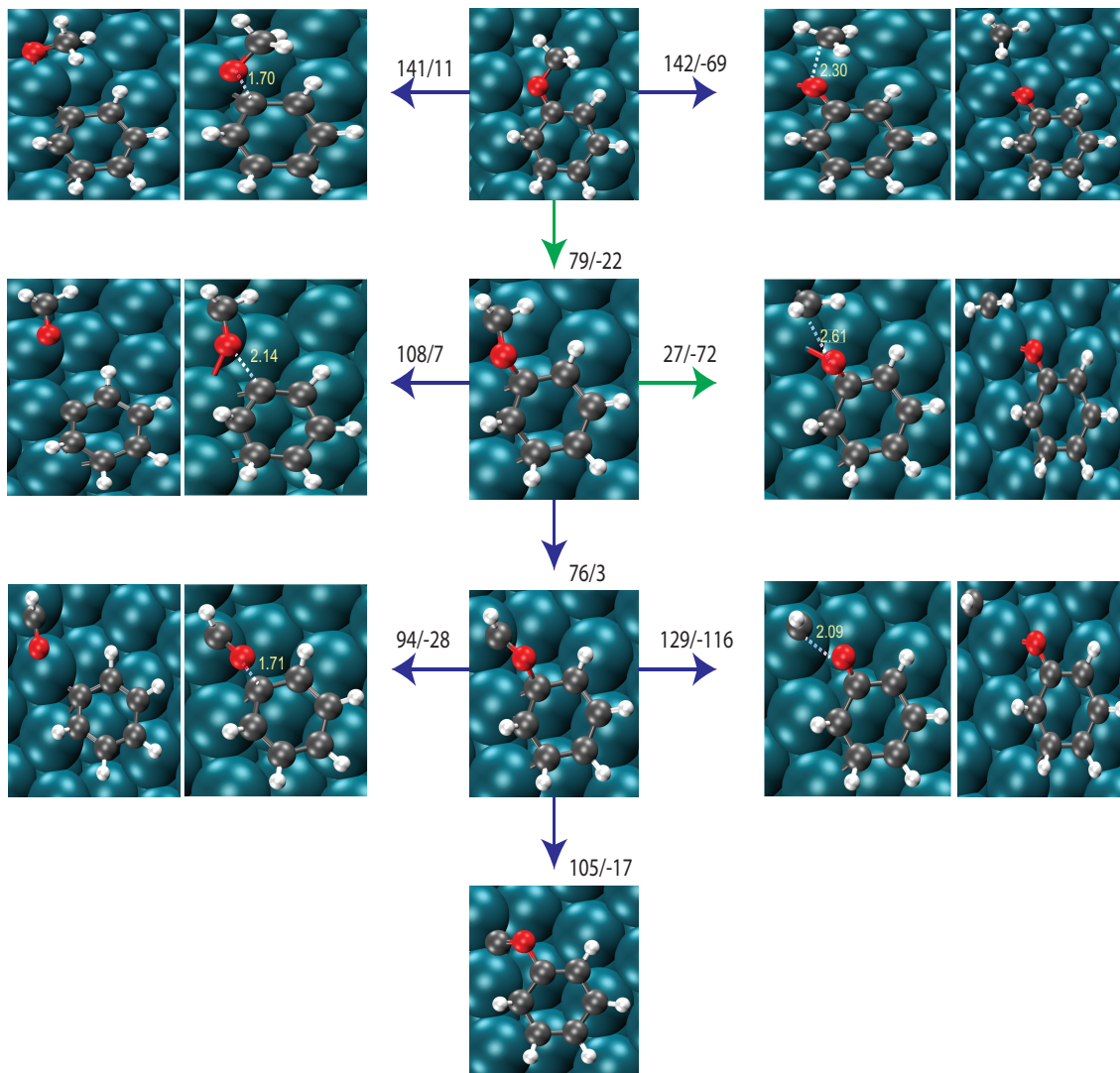Rh(111).

Figure 21. Layout of DFT calculated reactant, transition state and product structures for $C_{aromatic}$—O bond breaking, C_{alky}—O and dehydrogenation reactions of different Ph—O—CH_x ($1 \leq x \leq 3$) on stepped Rh(533) surface.

4.2.3. Note about direct of the cleavage $C_{aromatic}$—O bond

Direct cleavage of $C_{aromatic}$—O bond of anisole has been unfavorable both surfaces

Rh(111) and Rh(533), and in previous studies on Pt(111), Ru(0001), Fe(110). We

postulate that this is because the C in ($C_{aromatic}$—O) is sp2-hybridized, and the lone pair

of electrons on oxygen is under resonance with the 6-member ring. Attempts to break

this aromaticity would destabilize the conjugation and resonance (π-donation). Despite

the "inductive effect" or "taking away" effect of oxygen from less electronegative

carbons, oxygen in anisole has a "giving side". Since the oxygen is adjacent to a π-

bond, it will hybridize a pair of electrons with the π-bonds, as shown in Fig. 22.

Additionally, (—OCH$_3$) group is an ortho/para-directing group, and tends to push any

attacks near it away towards mostly para-postions of the benzene ring. Breaking this

aromaticity is almost always the rate-limiting step in aromatic reactions. This enhanced

stability renders the cleavage of $C_{aromatic}$—O very challenging. Fig. 22 shows the four

resonance structures from which, methoxybenzene (anisole) derives it stability.
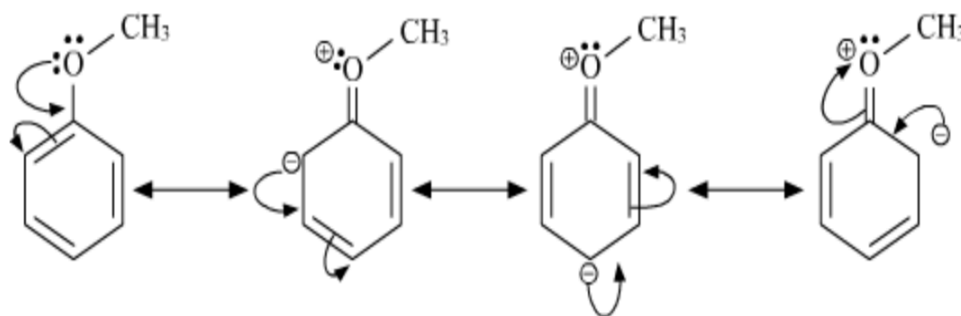
Figure 22. Resonance structures of anisole [51]

4.3. Fate of phenoxy intermediate

Once anisole has been sequentially dehydrogenated, a surface phenoxy remains as a

very vital intermediate.
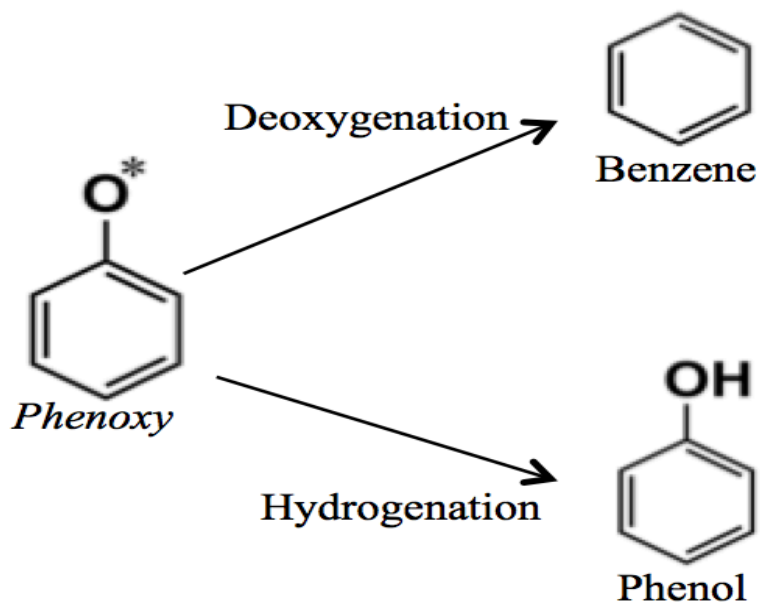
Figure 23. Proposed pathway fate of *surface phenoxy* intermediate
on Rh(111) and Rh(533)

As shown in Fig. 23, this intermediate can undergo either hydrogenation to form

phenol or a direct $C_{aromatic}$—O cleavage to form surface phenyl that needs

hydrogenation to become benzene.
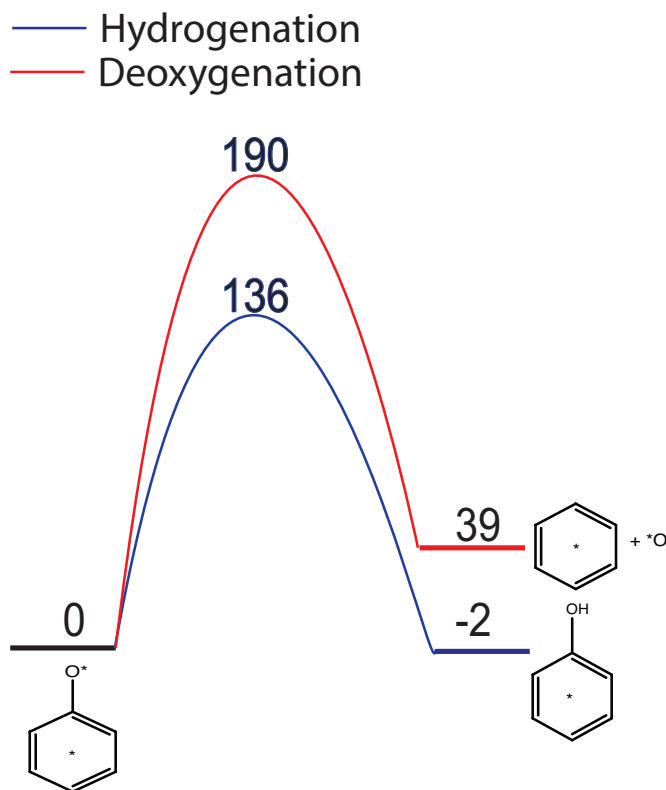
Figure 24. Energy diagram Rh(111) deoxygenation and hydrogenation of Ph-O*.

Experiments carried out by Pasco *et al.* showed that activation barriers for adsorption

of hydrogen on (111), (100), (110) surfaces of Fe were very small averaging at 48

kJ/mol [52]. Therefore, the actual surface reaction of hydrogenation of the phenoxy

(Ph—O*) intermediate to phenol was considered as rate limiting. As shown in Fig. 24,

the hydrogenation of phenoxy is exothermic on Rh(111) while it is significantly

endothermic on Rh(533). The energy barrier to hydrogenate the surface phenoxy is 136

kJ/mol less than that for deoxygenation on Rh(111) of 190 kJ/mol. This explains why

in experimental results, phenol was the main product of the surface phenoxy on Rh(111) surface. However, hydrogenation on Rh(111) is less favorable than previous studies on Pt(111) which was just 17 kJ/mol, and about the same as Ru(0001) of 134 kJ/mol, but less than that on Fe(110) of 147 kJ/mol.

Figure 25. Side view and top views of DFT calculated reactant, and product structures for deoxygenation/hydrogenation of phenoxy intermediate on Rh(111) terrace surface

The reaction scheme, shown in Fig. 25, outlines the DFT calculated reactants and product on the Rh(111) surface. The Rh—O bond length in phenoxy intermediate decreased from 2.98 Å in the original anisole (Rh—O) to 2.15 Å, in Fig. 25. The proximity of O* to the catalyst surface facilitated $C_{aromatic}$—O bond cleavage. Oxygen atom is located at a final distance of 3.01 Å away the phenyl ring.

4.3.2. Deoxygenation and hydrogenation on Rh(533)

As shown in Fig. 26 and 27, the hydrogenation of phenoxy is highly endothermic on

Rh(533) while it is exothermic on Rh(111). The energy barrier to hydrogenate the

surface phenoxy is 165 kJ/mol which is more than that for deoxygenation on Rh(533)

of 155 kJ/mol. This explains why benzene ratio to phenol increases more than it was

for Rh(111). Hydrogenation becomes increasingly difficult in order of Pt(111) to

Rh(111) to Rh(533).
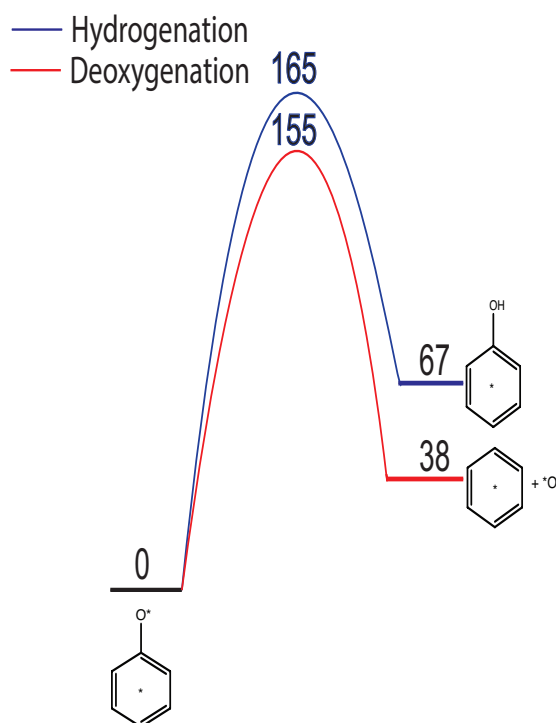
Figure 26. Energy diagram Rh(533) deoxygenation and
hydrogenation of Ph-O*

Deoxygenation on Rh(533) is less favorable than previous studies on Fe(110): - a

highly oxophilic surface, which had a barrier of 101 kJ/mol. But, it is more than

favorable to deoxygenate on Rh(533) than Ru(0001) which has a reaction barrier of 165 kJ/mol, and even more difficult on that on Pt(111) with a high barrier of 270 kJ/mol. Over the more oxophilic Rh(533) surface, the C—O cleavage is easier and this agrees with the trends of the energy barrier versus oxophilicity of different metals that we reported earlier as shown in Fig. 28.
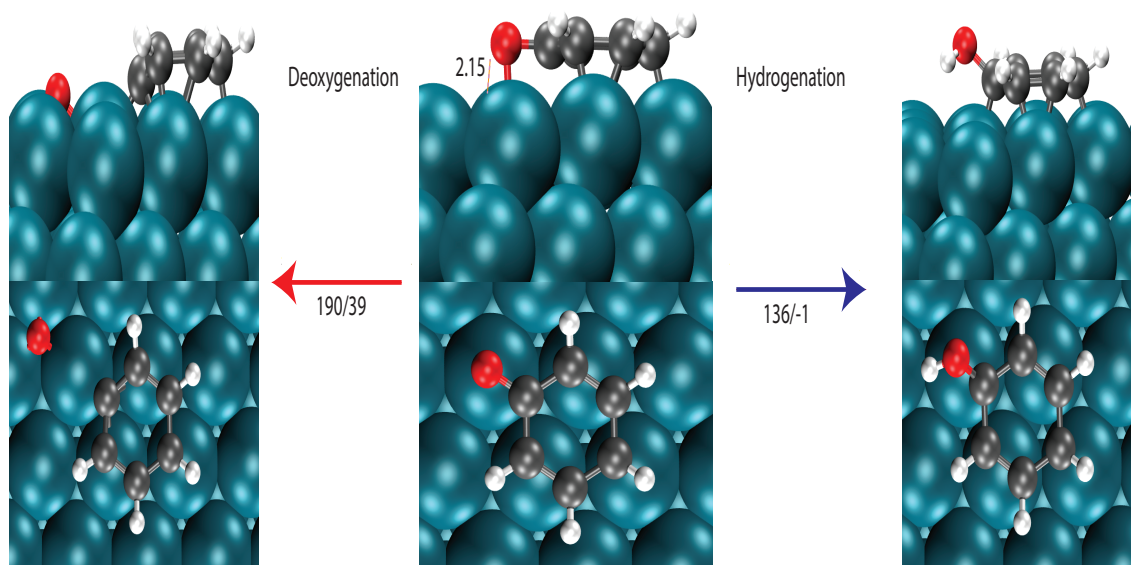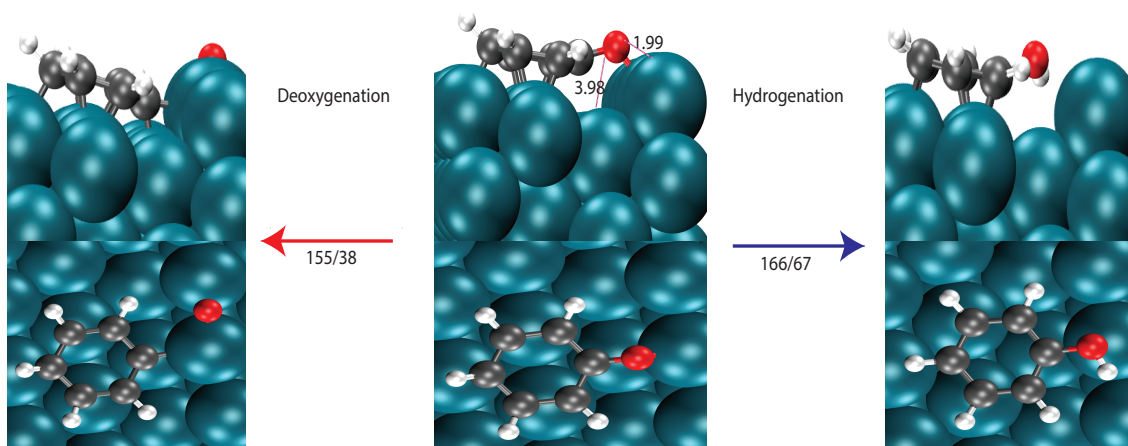

Figure 27. Side view and top views of DFT calculated reactant, and product structures for deoxygenation/hydrogenation of phenoxy intermediate

4.4. Adsorption energy as a catalytic descriptor

Unlike previous studies where both hydrogenation and deoxygenation were compared against oxophilicity together, in this study, I separated the two. Fig. 28 compares the deoxygenation pathway to oxygen adsorption (oxophilicity) and then Fig. 29 compares dehydrogenation to hydrogen adsorption on metal surfaces. We do not think oxophilicity can be a descriptor for hydrogenation because in one pathway, oxygen breaks and attaches to the surface, while in other hydrogen desorbs and attaches to

phenoxy. As shown in Fig. 28, the DFT calculated energy barreir for the

deoxygenation of anisole has a strong correlation with the oxophilicity (oxygen affinity

or adsorption) of the metal catalyst surfaces investigated in this study and also previous
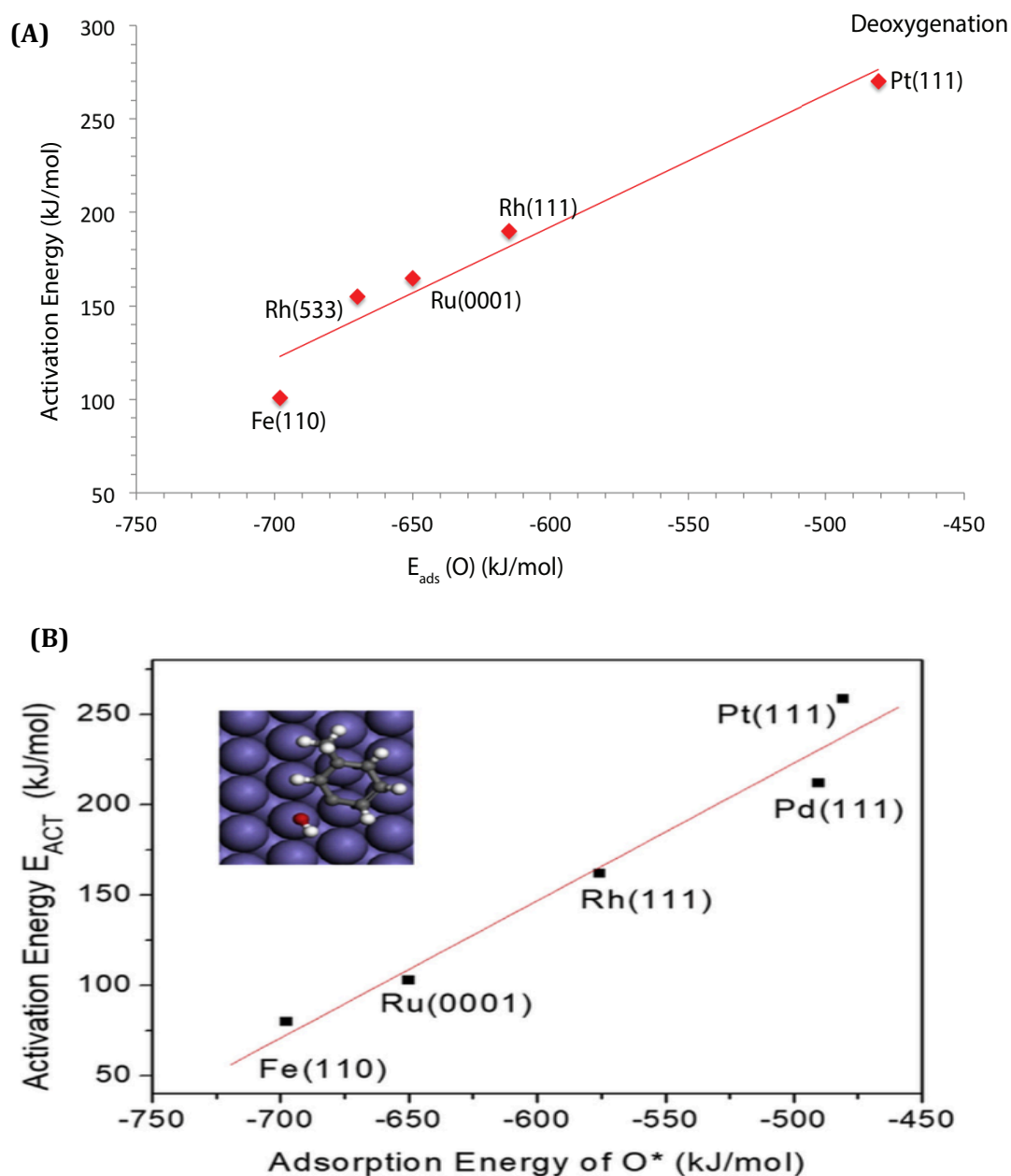
Figure 28. Correlation between activation energies for (a) deoxygenation of surface phenoxy (Ph—O*) on different metal surfaces and the oxophilicity (O-affinity). Modified from [5] (b) DDO of m-cresol, as comparison [11].

studies. Combining the two gives the correlation for deoxygenation versus oxygen adsorption in the order of: Pt(111) < Rh(111) < Ru(0001) < Rh(533) < Fe(110). The stronger the adsorption energy of atomic O atom on the surface, the easier it is to remove oxygen from a surface phenoxy, and adsorb it on metal surface.

Can we still use adsorption energy as a descriptor for catalytic activity for the case of hydrogenation reaction? As seen in Fig. 29, the activation barrier for hydrogenation of the surface phenoxy generally decreases, as the hydrogen adsorption energy decreases on the metal surface.
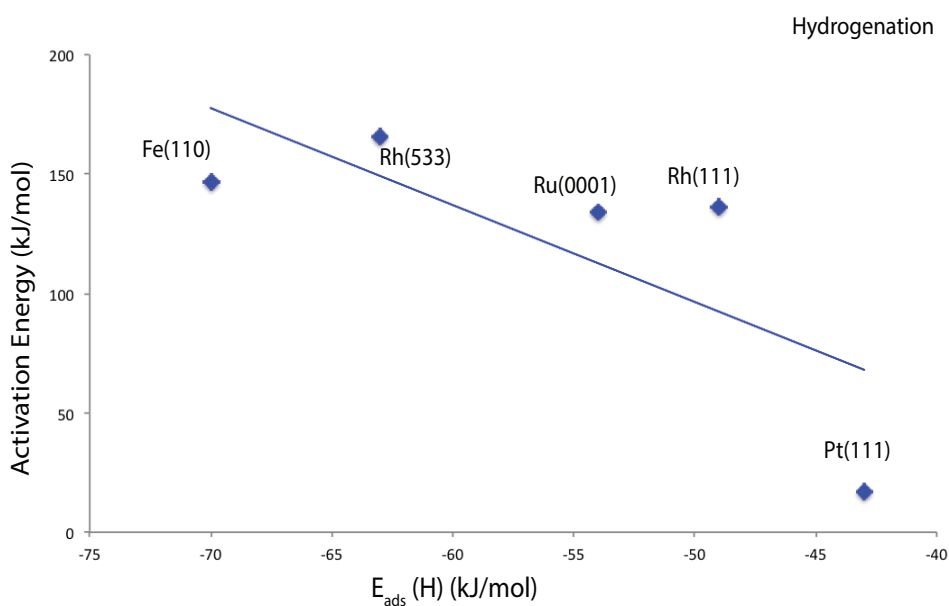
Figure 29. Correlation between activation energies for hydrogenation of intermediate Ph-O* on different metal surfaces and (H-affinity) on each of the metal surfaces. Modified from [5].

There isn't a perfectly linear correlation between hydrogenation and hydrogen adsorption energy compared to that for oxophilicity and deoxygenation. However, we can learn something from the trends. Pt(111) has the least atomic hydrogen adsorption energy of -43 kJ/mol and this explains the very low energy barrier of just 17 kJ/mol to hydrogenate the surface phenoxy.
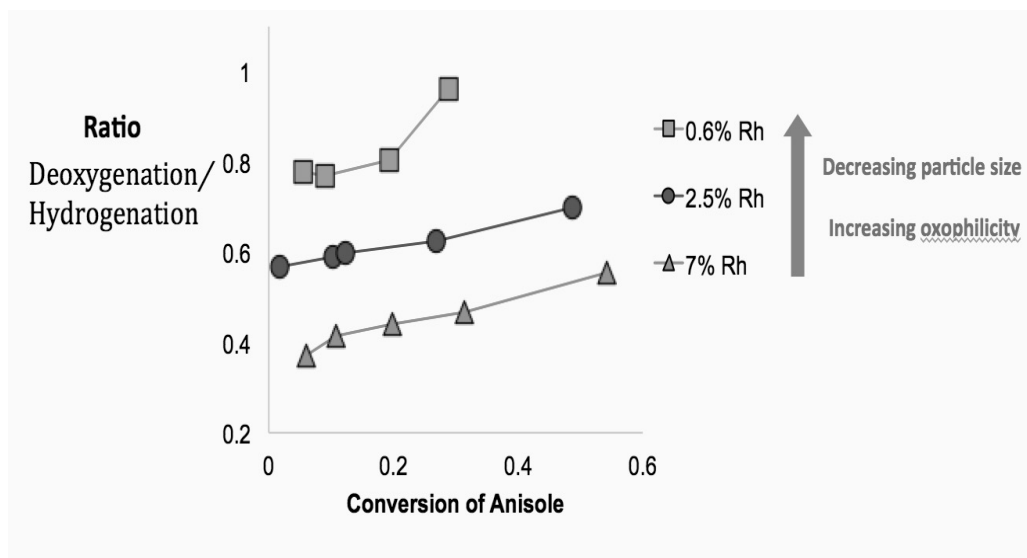
Figure 30: Experimental results as a corroboration with DFT studies. With permission from N. Duong.

This also explains why, despite the high price, platinum is a stable and effective catalyst for hydrogen evolution in fuel cells. However, other factors seem to influence hydrogenation energy barrier and not just its affinity on the metal.

According to experimental results, as shown in Fig. 30, we note that as the particle loading decreases, more deoxygenation takes place. Catalysts with smaller particle sizes catalysts increase the selectivity towards deoxygenation to form benzene, through

their increased oxophilic activity. It is also important to note, in Fig. 30, that the ratio

of deoxygenation to hydrogenation is still lower than unity, and this shows that phenol

is still the predominant product on the rhodium catalyst, but increasing particle size

allow more products of deoxygenation.

Table 5. Summary of the DFT calculated energetics (kJ/mol) of the elementary
steps in the HDO of anisole over the Rh(111), and Rh(533) surfaces.

Elementary steps		Rh111		Rh(533)	
		E_{act}	E_{rxn}	E_{act}	E_{rxn}
Dehydrogenation	Ph-O-CH3-->Ph-O-CH2*+H*	175	10	79	-22
	Ph-O-CH2*-->Ph-O-CH*+H*	91	-51	76	3
	Ph-O-CH*-->Ph-O-C*+H*	166	7	105	-17
C_{aryl}–O bond breaking	Ph-O-CH3*-->Ph* + *O-CH3	226	89	141	12
	Ph-O-CH2*-->Ph* + O-CH2*	196	47	108	7
	Ph-O-CH*-->Ph* + O-CH*	220	31	94	-28
C_{alkyl}–O bond breaking	Ph-O-CH3*-->Ph-O* + CH3*	258	-20	142	-70
	Ph-O-CH2*-->Ph-O* + CH2*	137	-36	27	-72
	Ph-O-CH*-->Ph-O* + CH*	143	-55	129	-116
Ph-O* intermediate	Ph-O* + H* --> Ph-OH	136	-1	166	67
	Ph-O* --> Ph* + O*	190	39	155	38

Chapter 5: Conclusion

Detailed studies were presented for the adsorption of anisole on Rh(111) and Rh(533)

surfaces using periodic DFT calculations. In addition, surface reactions for the possible

pathways of hydrodeoxygenation of anisole have also been discussed.

These results corroborated well with the results and trends that previous studies by Q. Tan *et al.* showed on Pt, Ru, and Fe close-packed metal surfaces. It was found that on all three metals, the dehydrogenation at the —OCH$_3$ side group is the most favorable reaction before any C—O bond breaking takes place. On both Rh(111) and Rh(533), the successive removal of the H atoms at the —CH$_3$ group facilitated the subsequent C—O bond breaking, especially the aliphatic C$_{alkyl}$—O breaking. C$_{aromatic}$—O remained difficult to break as reported before, and would require a highly oxophilic surface to directly cleave the bond to form benzene. Carefully designing the structure of the surface of the metal and modifying the electronic properties at the step, edges and terracewas found to control the selectivity of the catalyst. Steps on Rh(533) facilitated the hydrodeoxygenation of anisole towards more benzene, while Rh(111) led to more hydrogenation products such as phenol. This was explained by the shift and narrowing of the d-band towards the Fermi level on steps compared to terrace atoms. Finally, catalytic activity for deoxygenating anisole was found to follow the trend Pt(111) < *Rh(111)* < Ru(0001) < *Rh(533)* < Fe(110).

References

1. Sabatier, P., *Hydrogénations et déshydrogénations par catalyse.* European Journal of Inorganic Chemistry, 1911. **44**(3): p. 1984-2001.

2. Somorjai, G.A. and J. Carrazza, *Structure sensitivity of catalytic reactions.* Industrial & engineering chemistry fundamentals, 1986. **25**(1): p. 63-69.

3. Wang, H.L., M.Q. Feng, and B. Yang, *Catalytic hydrodeoxygenation of anisole: an insight into the role of metals in transalkylation reactions in bio-oil upgrading.* Green Chemistry, 2017. **19**(7): p. 1668-1673.

4. Perlack, R., et al., *US Department of Energy, Biomass as feedstock for a bioenergy and bioproducts industry: the technical feasibility of a billion-ton annual supply.* 2005.

5. Bridgwater, A. and G. Peacocke, *Fast pyrolysis processes for biomass.* Renewable and sustainable energy reviews, 2000. **4**(1): p. 1-73.

6. Di Blasi, C., *Combustion and gasification rates of lignocellulosic chars.* Progress in energy and combustion science, 2009. **35**(2): p. 121-140.

7. Sankaranarayanan, T.M., et al., *Hydrodeoxygenation of anisole as bio-oil model compound over supported Ni and Co catalysts: Effect of metal and support properties.* Catalysis Today, 2015. **243**: p. 163-172.

8. Moore, D., G.D. Robson, and A.P. Trinci, *21st century guidebook to fungi with CD.* 2011: Cambridge University Press.

9. Henkelman, G., B.P. Uberuaga, and H. Jonsson, *A climbing image nudged elastic band method for finding saddle points and minimum energy paths.* Journal of Chemical Physics, 2000. **113**(22): p. 9901-9904.

10. QIU, W.-h. and H.-z. CHEN, *Structure, Function and Higher Value Application of Lignin [J].* Journal of Cellulose Science and Technology, 2006. **1**: p. 010.

11. Klein, M. and P. Virk, *Modeling of lignin thermolysis.* Energy & Fuels, 2008. **22**(4): p. 2175-2182.

12. Chen, H., *Biotechnology of lignocellulose.* sl: sn, 2005: p. 73-141.

13. Zakzeski, J., et al., *The Catalytic Valorization of Lignin for the Production of Renewable Chemicals.* Chemical Reviews, 2010. **110**(6): p. 3552-3599.

14. Duong, N., Q. Tan, and D.E. Resasco, *Controlling phenolic hydrodeoxygenation by tailoring metal–O bond strength via specific catalyst metal type and particle size selection.* Comptes Rendus Chimie, 2017.

15. Yang, F.F., et al., *Size Dependence of Vapor Phase Hydrodeoxygenation of m-Cresol on Ni/SiO2 Catalysts.* Acs Catalysis, 2018. **8**(3): p. 1672-1682.

16. Tan, Q., et al., *Mechanistic analysis of the role of metal oxophilicity in the hydrodeoxygenation of anisole.* Journal of Catalysis, 2017. **347**: p. 102-115.

17. Sutton, A.D., et al., *The hydrodeoxygenation of bioderived furans into alkanes.* Nature Chemistry, 2013. **5**(5): p. 428-432.

18. Guvenatam, B., et al., *Hydrodeoxygenation of mono- and dimeric lignin model compounds on noble metal catalysts.* Catalysis Today, 2014. **233**: p. 83-91.

19. Goni, M.A. and J.I. Hedges, *Lignin Dimers - Structures, Distribution, and Potential Geochemical Applications.* Geochimica Et Cosmochimica Acta, 1992. **56**(11): p. 4025-4043.

20. Kepp, K.P., *A Quantitative Scale of Oxophilicity and Thiophilicity.* Inorganic Chemistry, 2016. **55**(18): p. 9461-9470.

21. Huang, X., et al., *Catalytic depolymerization of lignin and woody biomass in supercritical Ethanol: influence of reaction temperature and feedstock.* ACS sustainable chemistry & engineering, 2017. **5**(11): p. 10864-10874.

22. Si, Z., et al., *An Overview on Catalytic Hydrodeoxygenation of Pyrolysis Oil and Its Model Compounds.* Catalysts, 2017. **7**(6).

23. Tang, W.-w., et al., *Hydrodeoxygenation of Anisole over Ni/α-Al2O3 Catalyst.* Chinese Journal of Chemical Physics, 2016. **29**(5): p. 617.

24. Zhu, X.L., et al., *Bifunctional transalkylation and hydrodeoxygenation of anisole over a Pt/HBeta catalyst.* Journal of Catalysis, 2011. **281**(1): p. 21-29.

25. Wang, H., M. Feng, and B. Yang, *Catalytic hydrodeoxygenation of anisole: an insight into the role of metals in transalkylation reactions in bio-oil upgrading.* Green Chemistry, 2017. **19**(7): p. 1668-1673.

26. Chorkendorff, I. and J.W. Niemantsverdriet, *Concepts of modern catalysis and kinetics.* 2017: John Wiley & Sons.

27.	Chiusoli, G.P. and P.M. Maitlis, *Metal-catalysis in industrial organic processes.* 2008: Royal Society of Chemistry.

28.	Kitchin, J., et al., *Modification of the surface electronic and chemical properties of Pt (111) by subsurface 3d transition metals.* The Journal of chemical physics, 2004. **120**(21): p. 10240-10246.

29.	Robinson, A.M., J.E. Hensley, and J.W. Medlin, *Bifunctional catalysts for upgrading of biomass-derived oxygenates: a review.* ACS Catalysis, 2016. **6**(8): p. 5026-5043.

30.	Pichaikaran, S. and P. Arumugam, *Vapour phase hydrodeoxygenation of anisole over ruthenium and nickel supported mesoporous aluminosilicate.* Green Chemistry, 2016. **18**(9): p. 2888-2899.

31.	Asscher, M., et al., *The ammonia synthesis over rhenium single-crystal catalysts: kinetics, structure sensitivity, and effect of potassium and oxygen.* Journal of Catalysis, 1986. **98**(2): p. 277-287.

32.	Somorjai, G. and M. Yang, *The surface science of catalytic selectivity.* Topics in catalysis, 2003. **24**(1-4): p. 61-72.

33.	Lipkowitz, K.B. and D.B. Boyd, *Reviews in Computational Chemistry:* *Volume 13.* 2000: Wiley Online Library.

34.	Arblaster, J., *Journal Archive.* Platinum Metals Rev, 1996. **40**(2): p. 62.

35.	Jenkins, S.J., *Aromatic adsorption on metals via first-principles density functional theory.* Proceedings of the Royal Society a-Mathematical Physical and Engineering Sciences, 2009. **465**(2110): p. 2949-2976.

36.	Hoflund, G.B. and R.P. Merrill, *Molecular-Orbital Calculations of Atomic-Hydrogen Chemisorption on the Beryllium (0001) Surface.* Journal of Physical Chemistry, 1981. **85**(14): p. 2037-2041.

37.	Norskov, J.K., et al., *Trends in the exchange current for hydrogen evolution.* Journal of the Electrochemical Society, 2005. **152**(3): p. J23-J26.

38.	Yang, Q.Y. and C.L. Zhong, *Understanding hydrogen adsorption in metal-organic frameworks with open metal sites: A computational study.* Journal of Physical Chemistry B, 2006. **110**(2): p. 655-658.

39.	Saeys, M., et al., *Density functional study of benzene adsorption on Pt(111).* Journal of Physical Chemistry B, 2002. **106**(30): p. 7489-7498.

40. Kresse, G. and J. Hafner, *Ab initio molecular dynamics for liquid metals.* Physical Review B, 1993. **47**(1): p. 558.

41. Kresse, G. and J. Furthmüller, *Efficient iterative schemes for ab initio total-energy calculations using a plane-wave basis set.* Physical review B, 1996. **54**(16): p. 11169.

42. Perdew, J.P., K. Burke, and M. Ernzerhof, *Generalized gradient approximation made simple.* Physical Review Letters, 1996. **77**(18): p. 3865-3868.

43. Grimme, S., et al., *A consistent and accurate ab initio parametrization of density functional dispersion correction (DFT-D) for the 94 elements H-Pu.* Journal of Chemical Physics, 2010. **132**(15).

44. Henkelman, G. and H. Jónsson, *Improved tangent estimate in the nudged elastic band method for finding minimum energy paths and saddle points.* The Journal of chemical physics, 2000. **113**(22): p. 9978-9985.

45. Sheppard, D. and G. Henkelman, *Paths to which the Nudged Elastic Band Converges.* Journal of Computational Chemistry, 2011. **32**(8): p. 1769-1771.

46. Honkela, M.L., J. Bjork, and M. Persson, *Computational study of the adsorption and dissociation of phenol on Pt and Rh surfaces.* Physical Chemistry Chemical Physics, 2012. **14**(16): p. 5849-5854.

47. Watwe, R.M., et al., *Theoretical studies of stability and reactivity of C2 hydrocarbon species on Pt clusters, Pt (111), and Pt (211).* The Journal of Physical Chemistry B, 2000. **104**(10): p. 2299-2310.

48. Lovvik, O.M. and R.A. Olsen, *Adsorption energies and ordered structures of hydrogen on Pd(111) from density-functional periodic calculations.* Physical Review B, 1998. **58**(16): p. 10890-10898.

49. Pašti, I.A., N.M. Gavrilov, and S.V. Mentus, *Hydrogen adsorption on palladium and platinum overlayers: DFT study.* Advances in Physical Chemistry, 2011. **2011**.

50. Lopez-Moreno, S. and A.H. Romero, *Atomic and molecular oxygen adsorbed on (111) transition metal surfaces: Cu and Ni.* Journal of Chemical Physics, 2015. **142**(15).

51. Brouwer, D.M., E.L. Mackor, and C. Maclean, *Proton Magnetic Resonance Spectra of C-Protonated Anisole and 3,5-Dimethylanisole - Inhibition of*

Rotation About Partially Double C-O Bond - (Short Communication). Recueil Des Travaux Chimiques Des Pays-Bas, 1966. **85**(1): p. 114-&.

52.   Pasco, R.W. and P.J. Ficalora, *The Adsorption of Hydrogen on Iron - a Surface Orbital Modified Occupancy Bond-Energy Bond Order Calculation.* Surface Science, 1983. **134**(2): p. 476-498.